CHARACTERIZING DEFORMATION OF ISTANBUL WALL BY GEODETIC TERRESTRIAL LASER SCANNER

by

Maryna Batur

B.S., Mine Engineering, National Mining University of Ukraine, 2008

Submitted to Kandilli Observatory and
Earthquake Research Institute in partial fulfillment of
the requirements for the degree of
Master of Science

Graduate Program in Geodesy
Boğaziçi University

2020

To Murat Batur

ACKNOWLEDGEMENTS

Having transferred from being a graduate applicant to become a Master candidate, I would like to thank the authorities of Kandilli Observatory and Earthquake Research Institute for making this arrangement possible. In this respect I especially want to thank my Master thesis supervisor Prof. Dr. Haluk Ozener for his support and continuous assistance. I wish to express my appreciation to my co-supervisor, Dr. Onur Yilmaz, who showed the great interest to the topic of my thesis. You definitely the excellent supervisors and it was a great pleasure for me to be Your student.

I warmly thankful to Dr. Asli Sabuncu who patiently listened to all the ideas and problems that arose during my study and always came up with very useful suggestions.

Special thank I want to give to Mr. Hasan Bal from FARO Turkey company for his technical assistance in all my experimental work and for spending many hours to teach me how to use the instrument and deal with data. In addition, I am thankful to Mr. Erkan Baygul from Paksoy Teknik Hizmetler ve Tic. Ltd. Şti for his valuable advises and help.

My thanks are also given to all the faculty members in the Geodesy department. In particular, Prof. Dr. Semih Ergintav, Assoc. Prof. Dr. Fatih Bulut, Asst. Prof. Dr. Tulay Kaya Eken, Mr. Bulent Turgut and Ali Ahmet Altin for sharing their knowledge and experience. I also particularly grateful to Assoc. Prof. Dr. Asli Dogru who gave me much valuable advices in the early stages of my thesis.

My thanks are also given to my parents and my parents-in-low. They share my duties in the family, for which I will forever feel obliged. And a special thank I would like to give to my twins, Melisa and Batuhan, for making me stronger and better.

Finally, I want to thank to my husband, Murat Batur, for bringing me here and for his great encouragement over the period of my study. He always strongly believed in my personal development. Dear Murat, without You this work would never have been possible.

ABSTRACT

CHARACTERIZING DEFORMATION OF ISTANBUL WALL BY GEODETIC TERRESTRIAL LASER SCANNER

Historical buildings are an integral element of human civilization and they play a big part in cultural heritages for the descendants. Turkey, as being the cradle of civilizations, hosts very important and valuable structures. These structures are exposed to deformations for various reasons. Classical geodetic monitoring is a key approach for years to detect the deformation behaviors of structures. However, with the advanced technology, modern geodetic instruments replaced the classical geodetic instruments. Terrestrial Laser Scanner is built on the approach of acquiring a high-density point clouds, which represents X, Y, Z coordinates of the reflective surface. The case of Istanbul Land Walls has been chosen for this study due to its ~1600 years of historical value. In particular, two different towers of Land Walls having huge cracks on the front side of both structures is the motivation of this study. During this study, it happened an earthquake in Silivri offshore with the local magnitude (M_L) of 5.8. Thus, there are 2 observations before and after the earthquake. In total, three independent measurements are made. Data obtained from scanning were compared in Cyclone 3DR software using Cloud-to-Cloud method of deformation analysis. Geometries of structures are defined with outputs found by point clouds; deformation progresses are scrutinized, and three-dimensional models are constituted.

In conclusion, Terrestrial Laser Scanning technology is convenient to detect the deformations of historical structures with high capacity point clouds. The deformation maps obtained from comparing the point cloud data give a good structural information about the object by showing the current deformations and highlighting zones with possible future damage. It is thought that this study may provide a significant contribution to literature about not only protecting cultural heritage but also deformation studies.

ÖZET

YERSEL LAZER TARAMA TEKNİĞİ İLE İSTANBUL KARA SURLARININ DEFORMASYONUNUN BELİRLENMESİ

Tarihi yapılar, uygarlıkların ayrılmaz bir parçası olup, kültürel mirasın nesiden nesile aktarılmasında önemli rol oynamaktadır. Türkiye, medeniyetlerin beşiği olması nedeni ile sınırları içinde bir çok önemli ve değerli tarihi yapıyı içinde barındırmaktadır. Bu eserler zaman içinde çeşitli nedeni ile deformasyona uğramaktadır. Klasik jeodezik ölçme teknikleri, yapıların genel davranışlarını deformasyon belirlemede yıllardır başvurulan yöntemlerin başında gelmektedir. Ancak gelişen teknoloji ile birlikte jeodezik ölçme aletleri yerini güncel jeodezik aletlere bırakmıştır. Yersel lazer tarama teknolojisi, temel olarak hedef yüzeyinden X, Y, Z koordinatlarınıtemsil eden yüksek yoğunluklu nokta bulutu elde edilmesi üzerine çalışmaktadır. Bu tez çalışmasında, 1600 yıllık tarihsel geçmişe sahip olan Istanbul surlarının kara bölümü seçilmiştir. Kara surları üzerinde yer alan ve ön yüzeyinde derin çatlaklar bulunan 2 farklı burç çalışmanın ana motivasyonudur. Tez çalışması sırasında ayrıca Istanbul-Silivri'de orta büyüklükte bir deprem meydana gelmiştir. Çalışma bölgesindende gerçekleştirilen gözlemler bu sebeple deprem öncesi ve deprem sonrası olarak ayrılmıştır. Ölçmelerden elde edilen veriler Cloud to Cloud deformasyon analizi algoritması kullanılarak Cyclone 3 DR yazılımında değerlendirilmiştir.

Sonuç olarak, yersel lazer tarama teknolojisi tarihi yapılarda zaman içinde meydana gelen deformasyonları yüksek kapasiteli nokta bulutları sayesinde tespit edebildiği düşünülmektedir. Karşılaştırılan nokta bulutu verilerinden elde edilen deformasyon haritaları, mevcut deformasyonları ve ilerde zarar görebilecek belirli bölgeleri göstererek yapılar hakkında değerli yapısal bilgiler içermektedir. Bu çalışmanın hem deformasyon çalışmaları hem de kültürel mirasın korunması konularında literatüre önemli bir katkı sağlayacağı düşünülmektedir.

TABLE OF CONTENTS

ACKNOWLEDGEMENTS iii
ABSTRACT iv
ÖZET v
LIST OF FIGURES ix
LIST OF TABLES xvi
LIST OF SYMBOLS xviii
LIST OF ACRONYMS/ABBREVITATIONS xxi
1. INTRODUCTION 1
1.1. Overview 1
1.2. Research Objectives and Methodology 2
1.3. Literature Review 4
1.4. Scope of the Study 8
2. TERRESTRIAL LASER SCANNING TECHNOLOGY 9
2.1. Historical Development of Terrestrial Laser Scanners 9
2.2. Measuring Principle of Terrestrial Laser Scanners 10
2.2.1. Time-of-Flight 11
2.2.2. Phase-Shift 11
2.2.3. Triangulation 12
2.3. Coordinate System of Terrestrial Laser Scanner 13
2.4. Error Sources in Terrestrial Laser Scanners 14
2.4.1. Instrumental Related Errors 15
2.4.1.1. Laser Beam Propagation 15
2.4.1.2. Range and Angular Uncertainty 16
2.4.1.3. Axes Errors 17
2.4.1.4. Mixed Edge Problem 18
2.4.2. Object Related Errors 19
2.4.3. Environmental Errors 19
2.4.4. Methodological Errors 20
2.5. Areas of applications of Terrestrial Laser Scanners 20

2.5.1. Industrial Applications …… 21
2.5.2. Construction Industry and Civil Engineering Applications ……. 21
2.5.3. Architectural Applications for the Cultural Heritage Documentation and its Restauration ……..……..... 22
2.5.4. Geological Applications and Rockfall Studies …… 23
2.5.5. Mining, Tunnels, and Excavation Applications ……... 23
2.5.6. Disaster Monitoring Applications ……... 24
2.5.7. Transportation Projects ……... 24
2.5.8. Investigation of Landslides ……...…….. 25
2.5.9. Forensics Applications ……...……. 25
2.6. Advantages and Disadvantages of Terrestrial Laser Scanners …….. 25
3. TERRESTRIAL LASER SCANNING PROCEDURES …….. 27
3.1. Survey Planning …… 27
3.2. Data Acquisition ……...……. 30
3.3. Processing of Laser Scanning Data ……... 31
3.3.1. Registration …… 31
3.3.2. Georeferencing …… 36
3.3.3. Point Cloud Filtering ……..……. 37
3.3.4. Mesh Modeling ……... 39
4. GENERAL INFORMATION ABOUT DEFORMATIONS ……. 41
4.1. Definition and Types of Deformations ……. 41
4.2. Reasons of Deformations in Historical Structures …… 43
4.3. Standards for Deformation Monitoring …… 44
4.4. Methods of Deformation Analysis using Terrestrial Laser Scanning Technology…….. 47
4.4.1. Cloud-to-Cloud Method …….……..……...…… 47
4.4.2. Cloud-to-Mesh Method ……..……. 49
4.4.3. Mesh-to-Mesh Method ……..…….. 49
4.4.4. Error Sources in Deformation Analysis …….……. 50
5. APPLICATION ……..…….. 52
5.1. Case Study Area …….……... 52
5.1.1. History of the Case Study Area ……..……. 52

5.1.2. Seismicity of the Case Study Area ……. 54
5.2. Terrestrial Laser Scanner used in Application …….. 56
5.3. Process of Work ……...……..…… 58
5.3.1. Site Documentation ……...……..…… 58
5.3.2. Field Operations ……..…… 60
5.3.3. 3D Point Cloud Processing ……..…. 61
5.4. Deformation Analysis …….…….. 65
5.4.1. Deformation Analysis of Tower I …… 65
5.4.2. Deformation Analysis of Tower II …….. 68
6. CONCLUSIONS……..……. 70
REFERENCES …….…… 73

LIST OF FIGURES

Figure 1.1. Workflow of deformation analysis.……..……..……..…..... 2

Figure 2.1. First 3D scanners: (a) The RIEGL scanner; (b) The CYRAX scanner…….……..…… 9

Figure 2.2. Distance measurement in Time-of-Flight scanners…….…. 11

Figure 2.3. Distance measurement in Phase-Based scanners……..……..….. 12

Figure 2.4. Distance measurement in Triangulation scanning method…….…….. 13

Figure 2.5. Coordinate system of TLS……..…….……. 14

Figure 2.6. TLS's errors…….……..……... 15

Figure 2.7. Laser beam propagation…….……...…….... 16

Figure 2.8. Axes errors in TLS (c_e – collimation error; i – horizontal error)…….……...…….…… 18

Figure 2.9. Mixed edge problem……...……..…… 18

Figure 2.10. Beam divagation under the influence of bad environmental conditions……..…….……...…… 19

Figure 2.11. Range error due to incidence angle of laser beam (a_i – incidence angle)…….…… 20

Figure 3.1. Degree of time needed for the TLS procedure….……. 27

Figure 3.2. Types of targets: (a) Spherical target; (b) Marker; (c) Checkerboard.. 28

Figure 3.3. Line of sight with overlap…….…… 29

Figure 3.4. Scanning time based on the quality parameter…….……. 31

Figure 3.5. Workflow of coordinate transformation process……..……. 32

Figure 3.6. Types of coordinate systems: *SCS 1, 2, 3* – TLS' own Coordinate System related to its scan position; *LCS* – Local Coordinate System after the registration process; *NCS* – National Coordinate System after the georeferencing…….……..…….. 32

Figure 3.7. 3-D coordinate transformation…….……..... 33

Figure 3.8. Workflow of rigid transformation……..……... 36

Figure 3.9. Noise in data set: (A) and (C) shows noise because of wind and dust in the air; (B) shows noise probably resulting from hitting the sky with the laser beam; (D) represents noise due to movement of people……. 38

Figure 3.10. Point cloud project. Red rectangle represents the part of points that are needed for project deliverable……..……..……... 39

Figure 3.11. The process of 2D meshing by means of triangles…….……... 40

Figure 4.1. Stress-strain curve…….……... 41

Figure 4.2. Types of stresses: F – force, linearly applied on the object; M – force that causes bogy to rotate…….……. 42

Figure 4.3. Reasons of deformations in historical buildings…….……. 43

Figure 4.4. Workflow of deformation monitoring…….……. 45

Figure 4.5. Determination of deformation: (a) Deformation of the object after the two time periods; (b) Determination of geodetic points coordinates and the vectors of deformation……. 47

Figure 4.6. Basic concepts of C2C distance computation…….……. 48

Figure 4.7. Workflow showing principle steps required in C2M method……...…… 49

Figure 4.8. Workflow showing principle steps required in M2M method……...…… 50

Figure 5.1. The map of Historical Peninsula showing Land Walls, Sea Walls and Golden Horn Walls (Turnbull, 2012)…….……... 52

Figure 5.2. Land Walls of Istanbul: (a) Sections of the Land Walls after their construction (Turnbull, 2012); (b) Current state of Land Walls……..…….. 53

Figure 5.3. The case study area – location of towers on the map of Istanbul…..... 54

Figure 5.4. Historical earthquakes of Marmara region in the period of 400 – 1900 years given by Ambraseys (2002) and by Ambraseys and Jackson (2000)…….…….… 55

Figure 5.5. Historical earthquakes of Marmara region in the period of 1900 – 2019 years given by "KOERI-Regional Earthquake-Tsunami Monitoring Center" (KOERI, 2019); yellow color shows earthquakes with Mw 5 – 6; purple color shows earthquakes with Mw 6 – 7; red color shows earthquakes with Mw≥ 7……..……. 55

Figure 5.6. Istanbul-Silivri earthquakes and aftershocks: blue star – earthquake that occurred on 24th September 2019; yellow star - earthquake that occurred on 26th September 2019; red circles indicate aftershocks… 56

Figure 5.7. TLS FARO Focus 330 HDR (FARO Laser Scanner Focus 330 Manual, 2015)……... 57

Figure 5.8. Results of reconnaissance (distances are shown in meters)……. 58

Figure 5.9. The surroundings of study area: (a) Tower I; (b) Tower II……... 59

Figure 5.10. The surroundings of tower I from the East (taken from Google Earth)……..….. 59

Figure 5.11. Spherical targets……..…. 60

Figure 5.12. The process of scanning: (a) Tower I; (b) Tower II……...…... 61

Figure 5.13. Point cloud data before and after the target-based registration: (a) Tower I; (b) Tower II……..……..... 62

Figure 5.14. Single epochs and results of their registration: (a) Tower I; (b) Tower II……..…….. 63

Figure 5.15. Process of point cloud filtering by means of clipping box: (a) Tower I; (b) Tower II……..….. 64

Figure 5.16. Deviation maps of tower I with areas of change highlighted (A, B, C, and D): (a) 1. Period comparing; (b) 2. Period comparing……. 66

Figure 5.17. Percentage distribution of deviations in C2C analysis of tower I……...…….……. 66

Figure 5.18. The distribution of displacements in the highlighted areas of tower I: (a) area A, (b) area B, (c) area C, and (d) area D……... 67

Figure 5.19. Deviation maps of tower II with areas of change highlighted (A, B, C, and D): (a) 1. Period comparing; (b) 2. Period comparing…….….... 68

Figure 5.20. Percentage distribution of deviations in C2C analysis of tower II…… 68

Figure 5.21. The distribution of displacements in the highlighted areas of tower II: (a) area A, (b) area B, (c) area C, and (d) area D…..…….. 69

LIST OF TABLES

Table 2.1. Historical development of 3D scanners…… 10

Table 2.2. Comparison of scanning methods…… 13

Table 3.1. Distances from the scanner to the targets…….. 30

Table 3.2. Point distance and numbers of points……... 31

Table 3.3. Comparing of direct and indirect methods of georeferencing……... 37

Table 4.1. Classification of cracks in masonry building (Doshi et al., 2018)……. 44

Table 4.2. Geodetic techniques for deformation monitoring obtained from Kalkan et al. (2010) and Herban et al. (2014)……... 46

Table 5.1. Performance specifications of FARO Focus 330 HDR…… 57

Table 5.2. Date of data acquisitions…….. 60

Table 5.3. Target statistics for the tower I……. 62

Table 5.4. Target statistics for the tower II…… 62

Table 5.5. Scan statistics of epoch I, epoch II and epoch III…… 63

LIST OF SYMBOLS

a	Angle between the *ON* and the *XY*-Plane
a_A	Points of set A*p*
a_i	Incidence angle
A	Area
A_p	{1, 2, 3} set of 3D point clouds
b	Angle between *X*-Axis and the projection of *ON* onto the *XY*-Plane
b_B	Points of set B*p*
B_p	{1′, 2′, 3′} set of 3D point clouds
c	Speed of light
c_e	Collimation error
C	Centroid of point cloud data set
d_C	Distance computed by C2C method
d_G	Error after the georeferencing
d_N	Error due to noise presence
d_R	Error after the registration
$d\ (a_A, b_B)$	Euclidean distance between a_A and b_B
D	Distance from TLS to the object
D_1	Deformation of the 1. Period
D_2	Deformation of the 2. Period
D_{max}	Maximum deformation value
DEV_{3D}	3D deviation
D_S	Distance to the surface
f	Frequency
f_e	Effective position of the laser spot
F	Force, linearly applied on the object
$h\ (A_p, B_p)$	Hausdorff distance
H_0	Null hypothesis
H_1	Alternative hypothesis

i	Horizontal error
I	Initial vector
kg	Kilogram
km	Kilometer
L	Original length of the object
L_o	Length after the applied force
m	Meter
mm	Millimeter
mrad	Milliradian
M	Force that causes bogy to rotate
M_L	Local magnitude
M_w	Moment magnitude
nm	Nanometre
R	Rotation vector
S	Length of laser beam emitted from TLS to the target object
S_f	Scale factor
SNR	Signal to noise ratio
t	Time between sending and receiving the signal
T	Translation vector
T_b	Triangulation baseline
T_t	Pulse rise time
V_T	Transformed vector
w	The radius of the beam
w_0	The minimum beam radius (at the started point)
w_0^2	The squared minimum beam radius (at the started point)
$X_{meas}, Y_{meas}, Z_{meas}$	Planar coordinates of the compared frame
X_N, Y_N, Z_N	Polar coordinates of point cloud N
$X_{ref}, Y_{ref}, Z_{ref}$	Planar coordinates of the reference frame
δ_Z	The range uncertainty
δ_p	Uncertainty of laser position
ε	Strain

θ	Phase shift
λ	Laser wavelength
π	Pi value
ρ_w	Range relative to the beam waist location
σ	Stress

LIST OF ACRONYMS/ABBREVIATIONS

2D	2-dimentional
3D	3-dimentional
A.D.	Anno Domini
C2C	Cloud-to-Cloud
C2M	Cloud-to-Mesh
CRP	Close-Range Photogrammetry
DCRP	Digital Close-Range Photogrammetry
EDM	Electronic Distance Measurement
GNSS	Global Navigation Satellite System
GPS	Global Positioning Systems
ICP	Iterative Closest Point
InSAR	Interferometric Synthetic Aperture Radar
KOERI	Kandilli Observatory and Earthquake Research Institute
LCS	Local Coordinate System
LI	Laser Interferometry
M2M	Mesh-to-Mesh
NCS	National Coordinate System
PGL	Precise Geometric Levelling
SCS	Scanner Coordinate System
TIN	Triangular Irregular Network
TLS	Terrestrial Laser Scanning
TS	Total Station
UAV	Unmanned Aerial Vehicle
UNESCO	United Nations Educational, Scientific and Cultural Organization

1. INTRODUCTION

1.1. Overview

Historical sites and buildings play an important role in the human life, because they carry a long history and reflect the culture. It is an essential task that concerns the preservation and maintaining of the heritages for our descendants.

One of the forms of preservation is deformation monitoring, as it allows to assess and predict the behavior of the structure for safety reasons. Deformation monitoring is a complex issue and requires the use of definitive techniques which enable to provide an accurate spatial information of the structure. Usually, monitoring techniques are based on the use of simple geodetic methods. For example, deformation study by Total Station (TS) is shown in Kaloop *et al.* (2008) and Mill *et al.* (2013). Herban *et al.* (2014) used leveling to determine vertical displacement of the building. Meng *et al.* (2006) used Global Navigation Satellite System (GNSS) for the bridge monitoring. Lovse *et al.* (1995) performed dynamic monitoring of the tall structure by Global Positioning Systems (GPS) technique. Needless to say, that all these techniques have demonstrated obvious advantages and can be also used for the monitoring of historical buildings. However, they are narrowed to the study of individually selected points and sometimes do not give an opportunity to investigate the whole object.

With the improving of techniques, it is possible now to give a better insight into the complexity of the building by providing an accurate analysis of their structural conditions and thus, to indicate possibly critical deformations on earlier stages. One of these techniques is Terrestrial Laser Scanning (TLS), which allows to obtain a dense point cloud data on a high level of accuracy in a short period of time (Uray *et al.*, 2015). Several studies have been performed to investigate deformations of historical buildings using TLS and they are shown in the Chapter 1.3.

1.2. Research objectives and methodology

The aim of this study is to examine two towers of the Land Walls of Istanbul on deformations due to massive cracks on the front side of the structure. Initially, it was of interest to perform the deformation analysis based on two campaign of measurements. However, a medium intensity earthquake with the magnitude of M_w 5.7 occurred within the epicenter of approximately 60 km from the studied area. It is known that this earthquake was felt not only in the studied area, but also through the Marmara region and probably had a destructive impact on historical towers of this structure. This circumstance motivated to perform the third measurement and compare the results in order to see if there is an impact of earthquake. The workflow of the research is shown in Figure 1.1.

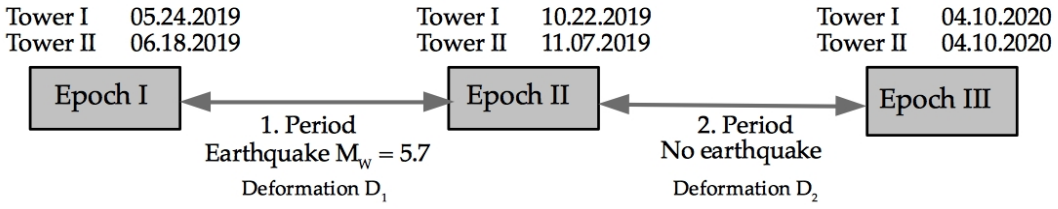

Figure 1.1. Workflow of deformation analysis.

To validate the assumptions that underline the question asked, the following hypothesis were verified:

1. Hypothesis H_0 (Null hypothesis): $D_1 = D_2$ – the value of deformation computed from the first and the second periods are identical. There is no impact of earthquake on the structure.
2. Hypothesis H_1 (Alternative hypothesis): $D_1 \neq D_2$ – the value of deformation computed from the first and the second periods are not identical. In this instance, two cases have place:
    - $D_1 > D_2$ – the deformation of the structure directly relevant to the earthquake;

- $D_1 < D_2$ – most probably there is other reason for deformation regardless of earthquake.

In order to interpret these values correctly, the time interval of the 2. Period was chosen to be the same as the time interval of the 1. Period.

Considering the situations described above, the main research objective was formulated: "Perform the deformation analysis of two towers of Land Walls using TLS point cloud data from three measurement campaigns and investigate the impact of earthquake on the value of deformation by comparing these data." In order to fulfil this research objective, the following questions were drafted:

1. How can TLS data be acquired properly?
2. How are collected data processed?
3. What are the limitations of processing and how these limitations may influence deformation analysis?
4. What are the available methods for deformation analysis using TLS technology?

The first question is answered by understanding the measurement principles of the TLS, by studying the main sources of errors in TLS, and by choosing the right scanning geometry.

One of the main steps of data processing is registration. The correct registration is necessary for deformation analysis. In this thesis, two methods of registration are explained in detail and showed graphically. This gives insight into the requirements on input data needed for deformation analysis and shows all possible limitations that may arise during the deformation analysis. Thus, the second and the third questions are answered.

Finally, the fourth question is answered by giving a clear description of all the available methods for deformation analysis. After answering all these questions, the research objective of the current thesis is considered to be accomplished.

The most interesting part of this study is that this investigation deals not only with current time deformations, but also with the deformations that have been occurring through centuries, because there has hitherto not been any restoration work in this part of Walls (Durusoy and Can, 2018). Some of the previous works were focused on the study of geology and microzonation of this area (e.g., Ince *et al*., 2008; Ince, 2012; Ündül and Tuğrul, 2006). Some studies were relied on the 3D modelling of Historical Peninsula (e.g., Dursun *et al*., 2008; Sengul, 2008; Kersten *et al*., 2009). Another work was carried out on the study of different mosque's minarets that are located in Historical Peninsula. These structures were studied on the behavior under earthquake loading (Oliveria *et al*., 2012). Kırlangıç *et al*. (2010) conducted the structural study of Land Walls and proposed a methodology that may prevent a collapse of the towers of Land Walls. Bayram *et al*. (2015) performed a digital recording of the Land Walls of Istanbul using two geodetic methods – TLS and Photogrammetry. The 3D model of the North façade of the Land Walls was computed and results obtained from two different methods were compared.

1.3. Literature review

In recent years there has been considerable interest in TLS Technology and numerous studies have been conducted to investigate deformations using this geodetic method. This section presents a review of recent literature concerning deformation analysis study using TLS.

Milli and Ellmann (2014), give an example of using TLS Leica Scan Station for the deformation monitoring of the suspension roof structure. The idea is to investigate the structural behavior of roof under the three different load conditions. Firstly, the object was scanned on its initial stage with no loads. The second scan was done when the roof covered with the layer of snow. Finally, the third measurement was performed after the snow was melt. Authors derived a 3D Triangular Irregular Network (TIN) surface models of each measured data and compared them using AutoCAD Civil 3D software. The comparing of the first and the second epochs showed that the roof has been deflected up to 60%. Comparison of the first and the third epochs showed that roof did not regained its original geometry and deflection was found as 72%.

Kanashin *et al.* (2017) describes the experience of applying TLS on reconstruction works of bridge in St. Petersburg. The main aim of this study was to create 3D models of external structural elements of the bridge and internal bridge equipment. These models were transformed into two coordinate systems, MSK-64 and Baltic Height system 77 respectively. The TLS Riegl was used for this work and as authors claimed, despite the huge number of irregular elements on the internal surface of bridge, it was possible to create a 3D model that represents all these complex structural features.

TLS technology has been widely investigated in deformation analysis of the dams. For example, Antova (2015) gives a brief overview of deformation monitoring of the dam. The Studena Dam (Bulgaria) was scanned by the Leica TLS twice – in December 2011 and in June 2012. The level of water known to be 832,81 m and 841,25 m respectively. Deformation analysis has been performed based on two methods of comparing, which are DEM-to-DEM (Digital Elevation Model) and Profile based methods. There was no evidence to suggest extreme values of deformations and only elastic deformations have been identified. According to the authors, these are due to water level in the dam.

Xu *et al.* (2019) applied TLS technology to the Changheba earth-rock dam. Authors performed registration using C2C registration method with the error of 2 mm. Deformation analysis was done by shortest distance comparison and results showed that deformations were mostly concentrated in the middle part of the dam.

Alba *et al.* (2006) performed a structural monitoring of Cancano Lake Dam in Italy. The main aims of this study were to investigate the accuracy of georeferencing and to perform a deformation analysis. For this, the large numbers of targets were used, and all measurements were done by two different instruments – Riegl and Leica. Deformations have been computed using four methods, which are mesh-to-points, polynomial surface-to-points, Mesh-to-Mesh (M2M), and polynomial surface-to- polynomial surface. Authors underlined that significant attention must be paid to the accuracy of georeferencing and to the method of comparison of point cloud data, because these have an impact on the final results. The authors also pointed out that TLS technology gives a possibility to derive a dense and accurate map of deformations.

Özdoğan and Deliormanli (2018) focused their attention on the different methods of deformation analysis. The underground drift of 30 m long was chosen for this study. Measurements were performed in two campaigns with the time intervals of 4 months using Leica Scanner. They used Cloud-to-Cloud (C2C), Cloud-to-Mesh (C2M), and section analysis, compared them and concluded that the first and the second methods show almost the same results, while the section method was quite distinct.

Bonali *et al.* (2014) traced the advances in TLS technology by investigating the historical building on deformations. The main focus of the experiment is to study if there were deformations due to earthquake. The object of this study is the ancient Church in Italy. First measurement was done in April 2011 and the second was carried out in June 2012, after the earthquake that struck in May 2012 with the magnitude of 5.0. Deformations were computed based on the differences between point clouds and this analysis showed very clear deviations maps, allowing to recognize the potential collapse of the structure.

Another deformation study of historical building was performed by Pellegrinelli *et al.* (2014). The historical Bell Tower (Italy) was taken under the geodetic monitoring due to weak settlement foundation and earthquakes risk. Firstly, the structure was monitored by levelling technique. After that, it was decided to perform the monitoring using the TLS technology and compare the results obtained from these two methods. Two scanning data were collected, before and immediately after the earthquake with the magnitude of 5.8. The results obtained from TLS validated the previous findings from levelling. The value of settlement was found as 0.5 mm per year with slow permanent movement of the structure.

In Ercan (2014), the deformation monitoring of historical Mihrimah Sultan Mosque was done using TLS technology. This study presented the detailed site surveying and data processing. Deformations were investigated based on ideal planes constructed from the point cloud data. As the results, deviations were found to be 3 cm for the main dome, 2 cm for the pendentives, and 5 cm for the piers.

In Vacca *et al.* (2016), three cases were presented on the study of damaged buildings. The first study concerns the historical Sivillier Castle. Here, authors focused on the

investigation of structural deformations. Based on the point cloud data, they created the Digital Surface Model and derived the contours from this model. The aim of the second study is to detect the displacements from the vertical axis of Bell Tower. Planimetrical dispersion of the various sections with respect to the ideal position was found. The third and the last case concerned the investigation of industrial building, that was partially damaged by the fire. From the 3D model it is easy to detect every detail and thus, damaged part was geometrically identified. In all cases, TLS technology showed the best results in obtaining the accurate 3D model with only one disadvantage mentioned by authors that is complex data processing.

The new method of estimation the deformations in heritage structure was proposed by Georgopoulos *et al.* (2016). The column of an ancient Temple in Greece, that was built in 330 BC, was chosen for this study. Firstly, the mesh surface was derived from the scanned data. After that, the column was divided into 13 drums and each part was analyzed separately. The center and the radius of each drum were calculated using known mathematical equations. These data were compared with the initial positions which are known from the previous surveys. As the result, column was found to move from its preliminary position on 0.066 m in South-West direction.

The similar research was done by Selbesoglu *et al.* (2016). The 386 years old historical mosque in Istanbul was chosen for this study due to the inclination of its minaret. The minaret was surveyed before using other geodetic methods differ from TLS and its geometry has already been identified. However, in order to study the relief of minaret and calculate the position of center of gravity, TLS technology was used. Based on the point cloud data, 31 sections with 30 cm interval each were created to identify the inclination. The first section was used as a reference frame in comparison with others. As the result, the total deformation on vertical plane was found to be 40,63 cm (taking into account that the height of the minaret is approximately 90 m).

1.4. Scope of the study

Chapter 1 introduces the problem, gives an overview about the study and describes its significance. This chapter also discusses the research objectives and methodology of the study. Moreover, the review of literature concerning the deformation monitoring using TLS technology are presented.

Chapter 2 provides an overview of TLS. It starts with the historical development of TLS. Further, measuring principles of TLS, sources of errors and main areas of applications are discussed. Finally, the advantages and disadvantages of TLS technology are presented.

Chapter 3 focuses on practical use of TLS. It begins with explanations of survey planning, continues with description of data acquisition, and ends with expression of data processing.

Chapter 4 discusses a theoretical knowledge about deformations, paying attention on the definition of deformation and its types. The main reasons of deformations in historical buildings are given. Much information is focused on the review of the methods of deformation analysis using TLS technology.

Chapter 5 introduces the case study. Study area is described in detail. The process of surveying planning, field operations, and data processing are explained. The final deliverables of the study in the form of deviation maps are given here.

Chapter 6 states the final results of the current study. Conclusions and further recommendations are given.

2. TERRESTRIAL LASER SCANNING TECHNOLOGY

Many different geodetic methods can be used for the deformation monitoring and for the characterizations of current deformations of the historical and heritage buildings. These methods are TS, Close Range Photogrammetry (CRP), Laser Interferometry (LI), GPS, Precise Geometric Levelling (PGL), but each of these tools comes with some limitations due to the size of building, adjusted area and complex elements in its design. TLS is a tool that can meet all these challenges. The main principle of its work consists of emitting the laser beam that is reflected from the scanned surface and return to the instrument. Distance can be estimated by the time-of-flight or by the phase difference. The result of the scan is millions of points with 3D coordinates that are called point clouds.

2.1. Historical Development of Terrestrial Laser Scanners

The first 3D scanner was developed in the last half of the 20th century with the aim to accurately recreate the surface of some object in the field of research and design. The company who was the first on the market cannot be determined exactly, but RIEGL (Austria) and CYRAX (USA) are known to be pioneers in this field (Mostafa Abdel-Bary Ebrahim, 2011). The Figure 2.1 shows the first TLS and the Table 2.1 represents a short historical development of TLS technology.



(a)



(b)

Figure 2.1. First 3D scanners: (a) The RIEGL scanner; (b) The CYRAX scanner.

Table 2.1. Historical development of 3D scanners.

Year	Description
1960	Due to limitations in equipment it took a lot of time to scan the object accurately
1985	There were some improvements in lights, but system still worked very slowly. The Cyberware laboratory in Los Angeles for the first-time used scanner to capture humans for animation industry.
1994	It was a significant breakthrough in laser technology. REPLICA scanner was developed that allowed for fast, detailed and accurate scanning.
1996	New scanners were able to capture the object with color just in a few minutes, but the instruments still were very bulky with external power supply and data storage. Typical representatives are CYRAX 2200 and RIEGL LMS Z210.
2002	First phase-based systems appeared on the market. Typical representatives are CYRAX 2500 and CALLIDUS.
2007	The range and the measurement speed were significantly improved in the new instruments. Data storage and the power supply are inside the instruments. Digital images are more and more combined with point clouds. Typical representatives are FARO PHOTON, RIEGL LMS Z420.
From 2010 till now	The data storage and power supply are fully integrated. The performance in terms of speed of measurements is improved and the range of measurements increases. Typical representative is FARO FOCUS.

2.2. Measuring Principle of Terrestrial Laser Scanners

TLS can be categorized into three categories based on the type of measuring the distance from the scanner to the object of interest. These are based on Time-of-Flight, Phase-Shift and Triangulation.

2.2.1. Time-of-Flight

The principle of Time-of-Flight distance measurement consists of measuring the time between emitted and reflected laser pulse (Hendriatiningsih *et al.*, 2015). Figure 2.2 represents the Time-of-Flight principle. The Laser Scanner sends the laser pulse to object, and when pulse is reflected from the object, it returns to the scanner. Distance is calculated by the Formula 2.1.

$$D = \frac{c.t}{2} \tag{2.1}$$

where

c: speed of light, c = 299 792 458 m/sec

t: time between sending and receiving the signal, sec

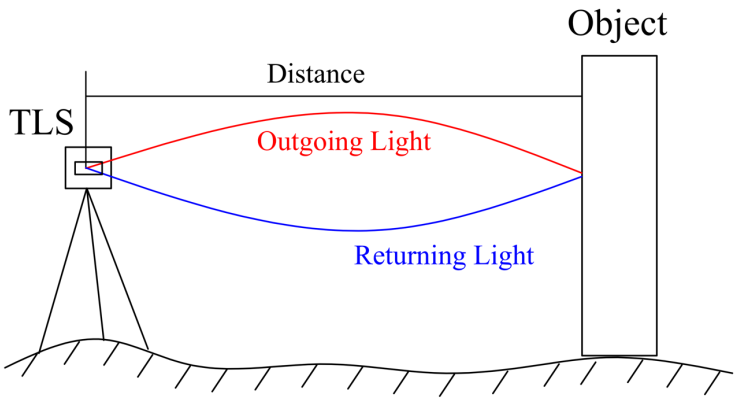

Figure 2.2. Distance measurement in Time-of-Flight scanners.

2.2.2. Phase-Shift

The main principle of Phase-Shift scanners is based on the measuring the phase shift of a pulse and distance is calculated along the sinusoidally modulated laser pulse (Romsek, 2008). The Figure 2.3 shows this principle of distance measurement.

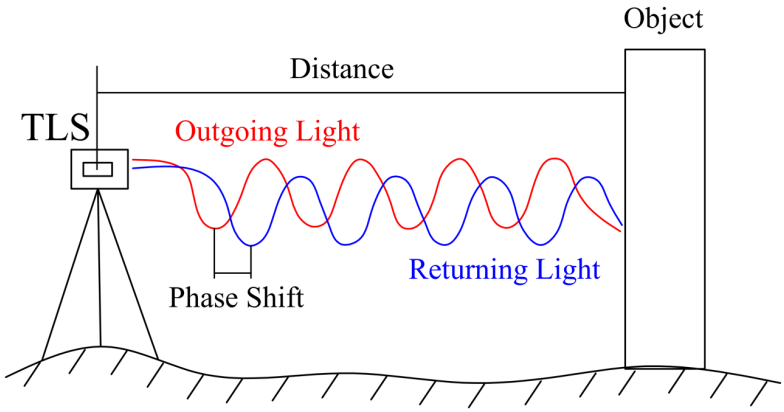

Figure 2.3. Distance measurement in Phase-Based scanners.

The distance from the scanner to the object can be defined from the Formula 2.2.

$$D = \frac{c.\theta}{4\pi f} \tag{2.2}$$

where

c: the speed of light

θ: phase shift

f: frequency

2.2.3. Triangulation

In Triangulation scanning method, scanner sends a laser dot to the object and uses the camera to determine the location of this dot. This method is called triangulation, because the laser, the camera and the dot form a triangle. One of the sides of a triangle is known and this is the distance between the camera and the laser. The angles b and c are also known. This information is enough to determine the dot (Abdelhafiz, 2009). Figure 2.4 shows the principle of triangulation scanning method. The Table 2.2 represents a summary of all the measuring principles listed above.

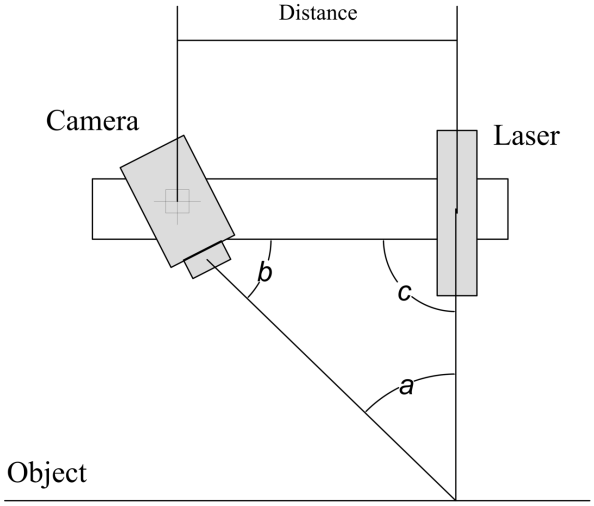

Figure 2.4. Distance measurement in Triangulation scanning method.

Table 2.2. Comparison of scanning methods.

	Time-of Flight	**Phase-Based**	**Triangulation**
Range	100 m and higher	Up to 100 m	Up to 10 m
Distance resolution	1 mm	0.1 mm	0.1 mm
Scan rate	Slow	Fast	Very fast
Commercially available scanners	Optech, Leica, Riegl, Trimble, Callidus	IQSun, Leica, FARO	Structured Light Pro S3, EinScan Pro 2X

2.3. Coordinate System of Terrestrial Laser Scanner

As mentioned in the previous paragraph, the principle of TLS work is based on the sending the laser beam, which is reflected from the surface and turn to the instrument, thus, recording the distance from itself to the object. The direction of laser beam is determined by two angles – vertical *a* and horizontal *b*, which are shown on the Figure 2.5. These measurements are performed in TLS' own coordinate system with the origin in the center of the scanners mirror. The coordinates (x, y, z) of each point cloud can be easily calculated by the Formula 2.3 (Kauker and Schwieger, 2017).

$$\begin{cases} x_N = S.\cos b\,.\cos a \\ y_N = S.\sin b\,.\cos a \\ z_N = S.\sin a \end{cases} \tag{2.3}$$

where

x_N, y_N, z_N: polar coordinates of point cloud N

S: length of laser beam emitted from TLS to the target object

a: angle between the ON and the XY-Plane

b: angle between X-Axis and the projection of ON onto the XY-Plane

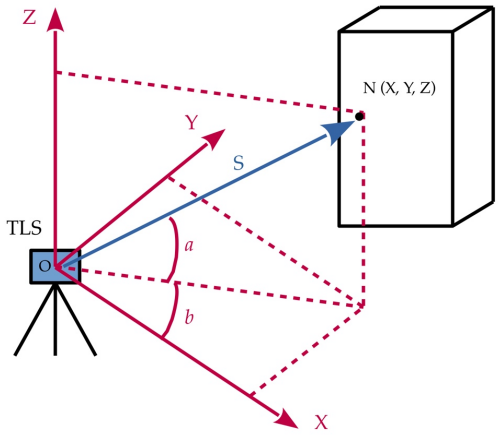

Figure 2.5. Coordinate system of TLS.

2.4. Error Sources in Terrestrial Laser Scanners

The result of TLS measurement is a point cloud data and the quality of data is given by the accuracy, that is the degree of agreement between a measurement and the conventional true value. In TLS, this is a coordinate accuracy of 3D points in point cloud.

No matter how accurate the instrument is, it will certainly contain measurement errors, depending on various factors. According to the prior researchers about the categorizing the error sources, for the TLS, four main categories can be defined that contribute to the quality of data (Gümüş, 2014). The classification of these errors is given on Figure 2.6. In addition

to the earlier studies, this chapter evaluates error sources by the three general types: random errors, systematic errors, and gross errors.

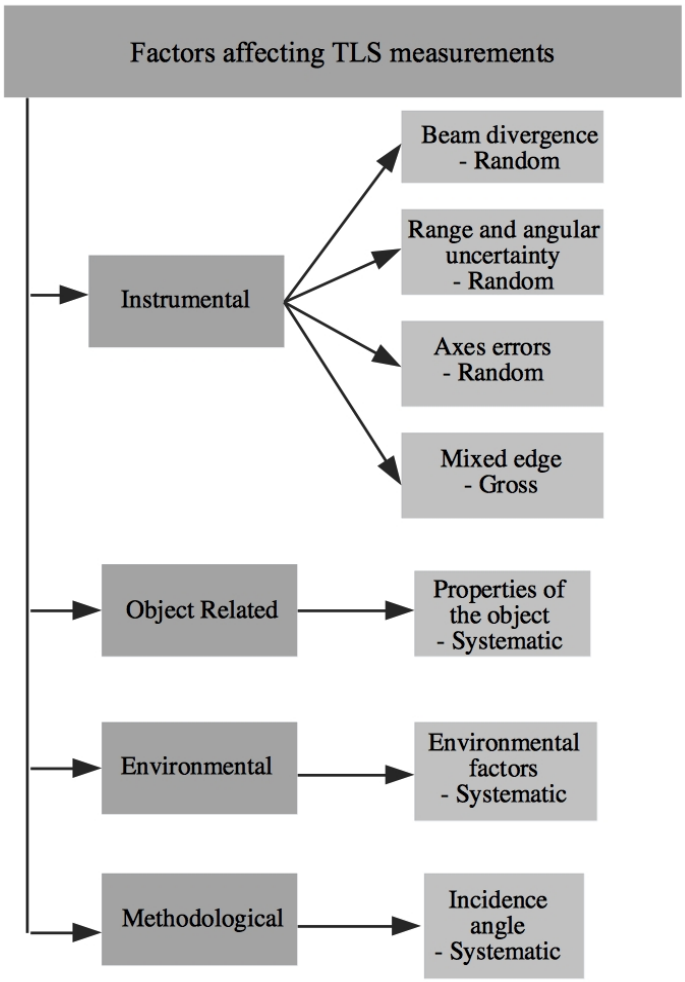

Figure 2.6. TLS's errors.

2.4.1. Instrumental Related Errors

2.4.1.1. Laser Beam Propagation. One of the main factors that influence cloud resolution is the beam divergence, which can be defined as the widening of laser beam and can be expressed by the Formula 2.4 (Jaafar, 2017):

$$w = w_0\sqrt{1 + \left(\frac{\lambda\rho_w}{\pi w_0^2}\right)^2} \tag{2.4}$$

where

w: the radius of the beam

w_o: the minimum beam radius (at the started point)

λ: laser wavelength

ρ_w: range relative to the beam waist location

Figure 2.7 shows the laser beam propagation. In order to overcome this problem, it is suggested to set up the instrument as close to the scanned object as possible.

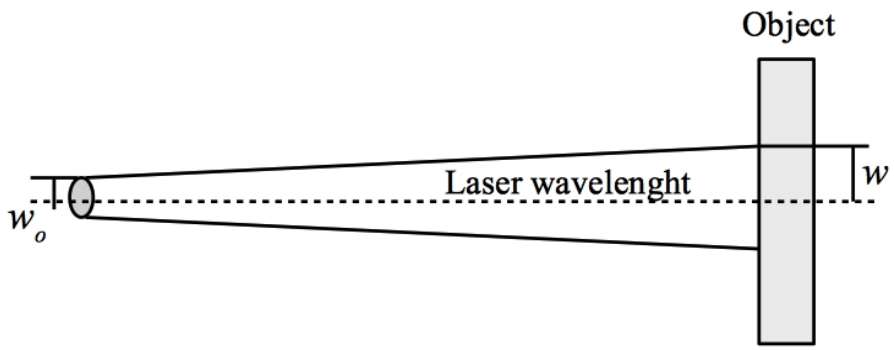

Figure 2.7. Laser beam propagation.

2.4.1.2. Range and Angular Uncertainty. The errors in range can be defined as a function of the parameters based on the type of TLS and its principle of work (Boehler *et al.,* 2003). Thus, for the time-of-flight scanners this error can be expressed by the Formula 2.5.

$$\delta_z \approx \frac{c.T_t}{2.\sqrt{SNR}} \tag{2.5}$$

where

c: speed of light

Tt: pulse rise time

SNR: signal to noise ratio

For the phase-shift scanners, the range uncertainty can be defined by the Formula 2.6.

$$\delta_z \approx \frac{\lambda_m}{4\pi.\sqrt{SNR}} \quad (2.6)$$

where

λm: modulated wavelength

Finally, for the triangulation laser scanners, the range uncertainty is calculated by the Formula 2.7.

$$\delta_z \approx \frac{{D_s}^2}{f_e.T_B}\delta_p \quad (2.7)$$

where

Ds: distance to the surface

fe: effective position of the laser spot

T_B: triangulation baseline

δp: uncertainty of laser position

As for the angular uncertainty, each TLS uses mirror to detect the beam in a particular direction. Some defects and imperfections of it introduces errors (Lee *et al*., 2016).

2.4.1.3. Axes Errors. Like many geodetic instruments, TLS have the three axes – vertical, horizontal, and collimation. These axes must be perpendicular to each other, but due to imperfections in manufacturing they may not be installed properly, thus, producing some errors in measurements (Reshetyuk, 2009). The Figure 2.8 shows the axes of TLS and errors due to their deviations.

Collimation error can be defined as angle between the collimation axis and the normal to the horizontal axis. Horizontal axis error is the angle between the horizontal axis and the normal to the vertical axis. Only the instrument calibration can address these deficiencies.

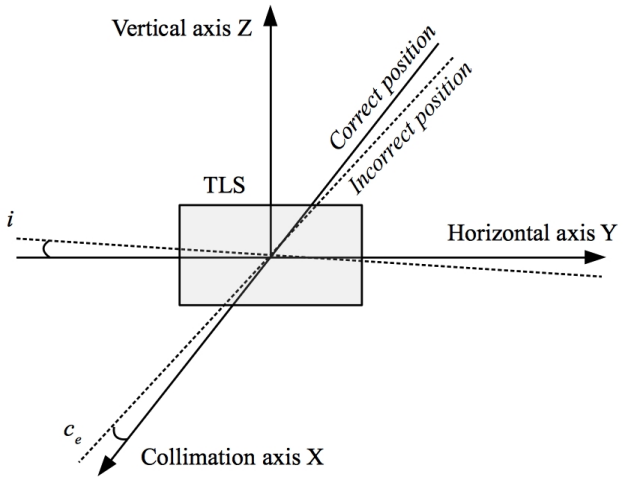

Figure 2.8. Axes errors in TLS (c_e – collimation error; i – horizontal error).

2.4.1.4. Mixed edge problem. These errors occur when measuring the object edges. When laser beam falls on the object edge, one part of it is reflected from the object, while another part is reflected from the surface that is adjusted to this edge or cannot be reflected at all. When receiver takes the laser beam, it does not identify the real location of the point and computes it by integration. It is shown by Jaafar (2017), this error in point position can vary from mm to several cm. Unfortunately, this error cannot be completely eliminated, but a way to overcome may be using TLS with a small beam divergence. Figure 2.9 illustrates the edge effects on measurements.

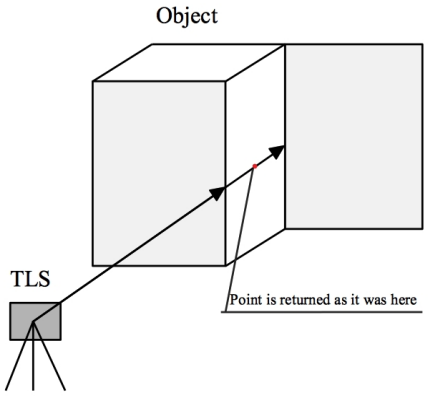

Figure 2.9. Mixed edge problem.

2.4.2. Object Related Errors

These cover errors related to the properties of object to be scanned. The primary source of error is the reflectivity of the object. Also, the following factors can relate directly to this type of errors:

- The surface color of object;
- Moisture of surface;
- Temperature of surface (for example, scanning hot objects in industrial environment);
- Surface roughness, etc.

The only way to overcome this is to use the same instrument for all scanning epochs and the same instrument settings (Jaafar, 2017).

2.4.3. Environmental Errors

These are environmental factors that affect the laser beam. For example, very hot temperatures and illumination may influence the emitted signal of laser beam. Besides, many TLS cannot operate under low temperatures. Such factor as humidity has an impact on the speed of light. Rain, dust and fog cause the reflection of the signal and the noise in data (Romsek, 2008). The way to correct the problem is not to perform measurements in adverse weather condition. Figure 2.10 shows the diversion of beam under the bad environmental conditions.

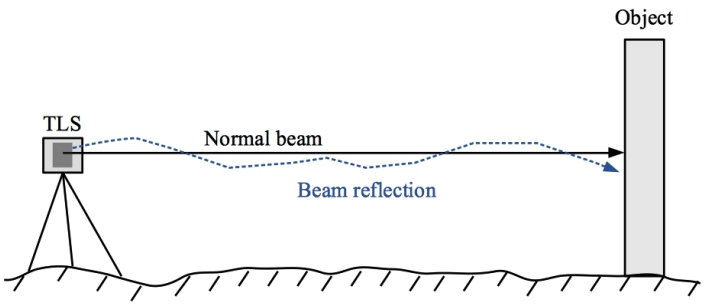

Figure 2.10. Beam divagation under the influence of bad environmental conditions.

2.4.4. Methodological Errors

These errors relate to the geometry of scanning. Unconscious configuration of survey method and wrong instrument position have an influence on incident angle, range and therefore on the point cloud density. Incidence angle can be defined as the angle between the laser beam and the normal to the scanned surface. The higher the incidence angle is, the higher size of the laser spot on the surface will be. Range error due to incidence angle is shown on the Figure 2.11.

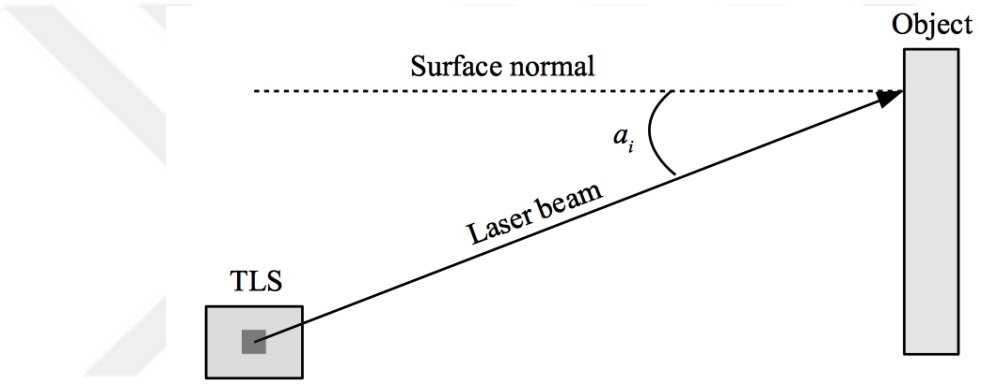

Figure 2.11. Range error due to incidence angle of laser beam (a_i – incidence angle).

The higher distance between the instrument and the object, the lower will be accuracy, because returned signal is weaker. As it was shown in experiments Soudarissanane *et al.* (2008) and Yaman (2013), the quality of point data is improved by moving the instrument closer to the scanned object. The way to prevent this error is to pay attention when choosing distance between the instrument and the object. According to Soudarissanane *et al.* (2007), the incidence angle should not exceed 75°.

2.5. Areas of Applications of Terrestrial Laser Scanners

Over the past decade, TLS technology has become very popular in many areas. For example, it is widely used by scientists and engineers in the following applications:

- Industrial applications;

- Construction industry and civil engineering;
- Architectural applications for the cultural heritage documentation and its restoration;
- Geological applications and rockfall studies;
- Mining, tunnels, and excavation applications;
- Disaster monitoring applications, such as earthquake studies;
- Transportation projects;
- Investigation of landslides;
- Structural health monitoring and deformation monitoring;
- Forensics applications, and many others.

2.5.1. Industrial Applications

One of the examples of industrial application is shown in Babic *et al.* (2011). Paper explains the process of surveying and measuring, as well as the procedure for modelling and creating a 3D visualization of the gas line. It is underlined by the authors that TLS provides a realistic representation of the object that can be easily understandable and analyzable. The only disadvantage is the data in the shape of point clouds is quite strenuous and requires knowledge of specialized software to handle with it. Another example is given in Bajtala *et al.* (2011). This article is focused on the use of TLS for the deformation monitoring in a factory chimney, to be more precise, for the determination of the tilt under the impact of sun radiation. For the validations of the results, measurements were also conducted using Total Station and as the results show, that there is a very little divergence in the coordinates that conform the following measurements.

2.5.2. Construction Industry and Civil Engineering Applications

3D laser scanning technology can be also used during the construction works. For example, scanning all the building elements after they have been installed provide the spatial information that can be compared to the design in order to verify that all components are placed according to the original project. This can be done with millimeter accuracy that makes possible to avoid errors or construction faults or, if such errors take place, to adjust them in short order. In addition, engineers use 3D data to determine the volume of necessary

construction material that leads to less waste. Besides, terrestrial laser technology is successfully adopted for moisture detection in building materials. As an example, Suchocki and Katzer (2018) discuss theoretical and practical aspects of TLS measurements for the detection of water presence. The article stresses factors that can enable or disable effective moisture detection. These are roughness and color of the structure. Despite some limitations, authors underlie the contribution of laser scanners in this task of civil engineering.

2.5.3. Architectural applications for the cultural heritage documentation and its restauration

Keeping heritages and their documentation is a very important step for their protections. TLS technology is also one of the most useful and appreciated among the engineers. As an illustration, Uray *et al.* (2015) demonstrate 3D architectural surveying of Diyarbakir Walls with terrestrial laser scanner. They explain the process of data acquisition with its further processing and, finally, explain the process of obtaining the 3D model of the given structure. Based on this 3D model, it is possible to compute a geometrical data of the structure such as profiles, views and plans. These are used by architectures for documentation purposes. TLS can be used not only for documentation of heritages, but also for the reconstruction of destroyed structures. Particularly, in Bitelli *et al.* (2017) there is an example of 3D virtual reconstruction of the civic tower (Italy) that was destroyed in 1944. The process of surveying and reconstruction are presented in this paper. The aim of this work was to create a 3D model of no longer existing building. Historical images have been used to provide the base from which 3D model was derived. In addition, authors compare 3D coordinates of the structure obtained from laser scanner and photogrammetry and these are with a satisfied accuracy. Thus, the TLS technology makes possible to reconstruct the ancient building. Another paper shows that laser scanners can be used to detect traces of restoration works. Pesci *et al.* (2012) addresses the Palazzo d'Accursio case study in Italy. Information obtained from TLS makes possible to create a high-resolution digital image for morphology analysis. The aim of which is to confirm the historical documentation about phases of construction. Authors also indicate that 3D scanning allows to construct a map that will point out all surface anomalies of the current historical structure.

2.5.4. Geological applications and rockfall studies

Several studies have been carried out on using the TLS technology in the field of structural geology. Abellan *et al.* (2006) focused on rock fall study. As a result, authors have obtained a high accuracy DEM, which allowed to obtain an accurate information on the detachment location, joint orientation and rockfall trajectories. In Abellan *et al.* (2010) the authors analyzed datasets from TLS and detected two types of mass movement. They also studied the displacement of likely slab failure and suggested stationary stage of it. Experiments on cliff monitoring were conducted by Rosser *et al.* (2005). A group of researchers had monitored a cliff on the coast of North Yorkshire, UK, for 16 months. Based on the acquired data, cliff face was displayed in contours which allowed to detect a pattern of erosion. And they reached the conclusion that TLS technology allows to obtain more full range of spatial information compare to traditional survey techniques.

2.5.5. Mining, tunnels, and excavation applications

3D scanners are also widely applied in the mining environment. For instance, the scientific paper Kajzar *et al.* (2017) is directed on the roadways and pillar stability monitoring using TLS. As authors say, this task is very important in geotechnical engineering and requires high accuracy. TLS technology was found as ideal for monitoring operations in mining. Here, authors give an example of 8 epochs of monitoring surveys. After they analyzed all the repeated scans, the conclusion was made that movement took place more than 600 mm. As the final point, authors confirm that TLS technology is able to identify the places of significant movements in all the details. As for the using of TLS in tunnels, there are two main types of its application here: deformation measurements and representation of geometrical features of the tunnels. The latter is used for accurate tunnel mapping. In Lam, (2006) there is an example of using laser scanner during the tunnel construction. In this study, author explains how to choose the right procedure for data acquisition and describe the algorithm of computing geometrical features such as profiles and surface views. Then, author compares them with the plan and may suggest about the degree of construction accuracy. In case of deformation measurements, many works were implemented in this study too. The examples are Delaloye *et al.* (2012), Han *et al.* (2013),

Lemy *et al.* (2006). According to these papers, deformation analysis usually to be divided into two parts. The first part concerns comparing the acquired tunnel data in several time periods, and the second part is comparing data from one of epoch with a designed model.

2.5.6. Disaster monitoring applications

3D digital models are also very useful in natural hazard and risk assessment study. Vasilakos *et al.* (2018) compare terrestrial photogrammetry to the laser scanner for the 3D mapping of damaged buildings after the earthquake with 6.3 magnitude that happened in Aegean Sea (Greece). According to this study, 3D model obtained from the TLS was much more accurate comparing to those obtained from photogrammetry. In addition, based on this method, agencies performed calculations of the property losses with the full representation of physical state of buildings after the earthquake. Also, data obtained from laser scanners can be used to investigate the postseismic surface deformations. As an illustration, in Kayen *et al.* (2006) scanner data were used to map the topography of the ground deformed by the earthquake and to study the current deformations and changes in surface. The authors underlie that 3D scanners allow precisely characterize a very complex surface features with detailed geometry in a short period of time. Because of possibility to obtain a 3D model of damaged ground, it is easy to evaluate a deformation potential. Karabacak *et al.* (2011) used ground-based LIDAR to study the surface creep along the North Anatolian Fault (NAF) at the IsmetPasa and Destek Sections. Three manmade walls that were constructed almost perpendicular to the fault line, were measured in the period from June 2007 and November 2009. The results from this study showed the creep rates of 6.8 – 10.0 ± 4.0 and 9.1 – 10.0 ± 4.0 mm/year at two sites near IsmetPasa and 6.0 – 7.2 ± 4.0 mm/year in Destek section.

2.5.7. Transportation projects

There are numerous studies focused on the use of TLS in transportation applications. For example, Slattery *et al.* (2012) created a 3D model before and after the road construction from the point cloud data. Based on this model, earthwork volume during the construction was easily calculated. In Jaselskis *et al.* (2005), several case studies have been conducted to investigate the use of TLS technology in road construction area. The first study was aimed

to the volume calculation of soil and rock. Second case was about the determination of surface elevations and bridge beam camber. The last study consisted in creation of as-build drawings in 3D representation. Authors reached the conclusion that the current technology can be effectively used in this field, allowing for safer and more accurate measurements compare to other survey methods.

2.5.8. Investigation of landslides

In landslides study, Teza *et al.* (2007) introduced a new method for the displacement calculation, based on the Iterative Closest Point (ICP) algorithm using TLS technology. They performed two tests – the first studied area was directly observable, and the annual displacement was found as 20 cm, and the second area was hidden for the direct observation (area represented a village) and the average displacement was found as 2 – 3 cm per year. Authors came to conclusion that this approach was successfully applied to the landslides study and allowed to detect a high-risk displacement.

2.5.9. Forensics applications

Nowadays, 3D scanners are widely used in the field of forensics. For example, the speed at impact during the car accident can be easily measured by interpretation the scanned documents of body deformation (Ebrahim, 2001). Also, during the crime scene study, TLS allows to capture the entire geometry of the crime place, as well as document some aspects of scene that may not be observed by naked eye at the first investigation (Komar *et al*., 2012).

2.6. Advantages and Disadvantages of Terrestrial Laser Scanners

There are many advantages in using TLS technology and they can be listed as:

- Possibility of use in all areas of industry, construction and architecture;
- Fast and accurate method of digitizing real objects;
- Being sure that all the necessary information has been collected, allowing to avoid risk of having to return to the site to integrate with new measures;

- No need to touch the measured object, which in some cases is not possible;
- High accuracy of measurements;
- Ability to represent the object in 3D representation in a true color image;
- Day or night operating;
- Indoor and outdoor scanning;
- Compare “designed model” to “build model”.

One of the major disadvantages of TLS technology is that data processing is quite long and complex. There is a need in highly specific software to process the scanned data. Another negative aspect is that cost of scanners and service fees are higher compare to manual surveying techniques. The last drawback to highlight is that the instrument is environmental dependent. In other words, it cannot be used in rainy or foggy weather.

3. TERRESTRIAL LASER SCANNING PROCEDURES

TLS is automated procedure; however, some steps require deep knowledge of scanning strategy and may take plenty of time and efforts. The stream of the entire work can be divided into three steps – survey planning, data acquisition and data processing. As practice shows, survey planning takes little time – from an hour to one day; data acquisition may be much more consuming, while data processing requires much time and can be lasted even a month. The Figure 3.1 shows operating time using TLS technology.

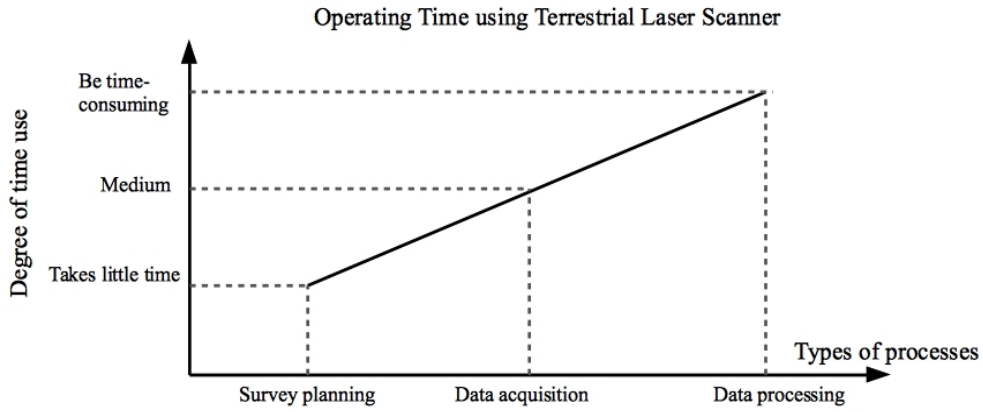

Figure 3.1. Degree of time needed for the TLS procedure.

3.1. Survey planning

One of the key issues before starting scanning, is to determine goals and objectives of the project. Two main questions are needed to be answered:

1. Why is object needed to be scanned?
2. What will final deliverables be?

Answers can provide insight on the requirements concerning instrument, accuracy and method of data acquisition. For example, if the goal of the study is to perform historical documentation, deliverables in this case are 2D architectural drawings or 3D mesh model of

the scanned structure. Deformation monitoring will end with deviation maps. The accuracy of point clouds in case of heritage study may not be very high, but for deformation analysis purposes the high accuracy of point clouds must be strictly observed.

The next step is the analyzing area to be surveyed. Gathering information about the structure that will be scanned and its surroundings can give a clear idea of work complexity and time required for scanning. Area can be scattered with obstructions, limiting fitting setup of instrument and targets. It is suggested to take field notes, sketches, make photographs or maps of building and its adjusted area.

The last step is to determine possible instrument and targets positions. TLS should be set up to guarantee a maximum coverage of building while minimizing the number of stand points. The line of sight must be clear with appropriate range. Next to the optimal instrument position, target types and their geometric configuration play an important role in the process of scanning. Targets are the artificial objects that may be in a variety of forms, for example, spheres, markers, or checkerboards and mainly used for registration purposes. They are usually manufactured by laser scanner companies and made from highly reflective materials. Markers and checkerboards are usually put directly on the structure, while spherical targets can be put on the ground avoiding physical contact with the scanned object. Types of targets are shown on the Figure 3.2.

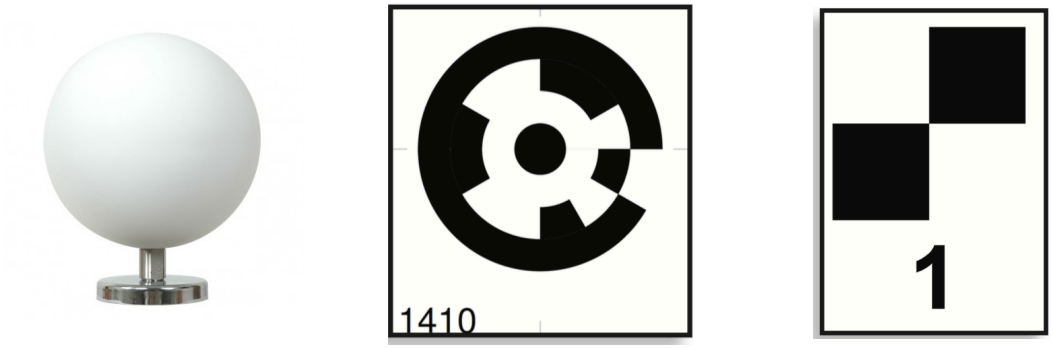

(a) (b) (c)

Figure 3.2. Types of targets: (a) Spherical target; (b) Marker; (c) Checkerboard.

The choice of targets depends on the type of structure and site conditions in some way. For example, in case of historical value of the structure it is likely prohibited to put checkerboards or marks on the walls directly. In this case, spherical targets may be used. Sometimes, neither markers nor spherical targets can be used. In such circumstances, scanning is performed without targets, but on the condition that at least 30% of point cloud overlap will be done as it is shown on the Figure 3.3 for refine registration.

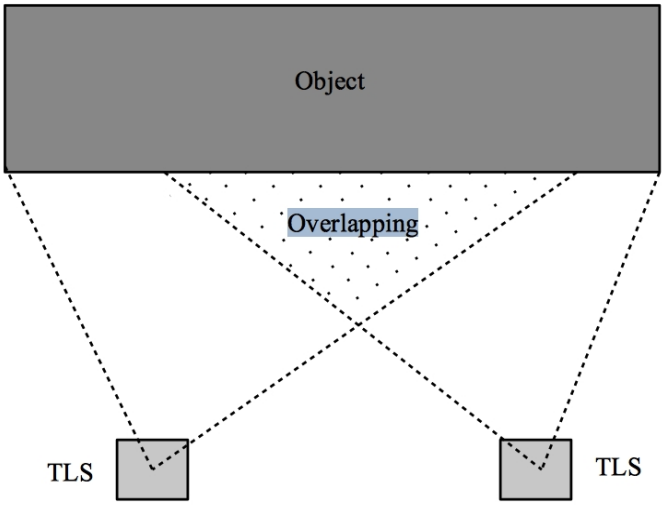

Figure 3.3. Line of sight with overlap.

There are some rules that should be taken into account when choosing geometric configuration of targets:

1. Targets should be widely spread not only in X and Y position, but also in Z-direction wherever possible.
2. At least three targets must be common for each scan for the good registration.
3. Distances from TLS to targets must comply with the requirements listed in instrument manuals.

For the TLS FARO Focus 330 HDR, maximum distances from the instrument to the targets depend on the scanner settings and are shown in the Table 3.1.

Table 3.1. Distances from the scanner to the targets.

Resolution setting	**Point distance mm at 10m**	**Maximum distance m**
1/16	24.54	4.5
1/10	15.34	7.5
1/8	12.27	10
1/5	7.67	12
1/4	6.14	19
1/2	3.07	39
1/1	1.53	70.5

3.2. Data acquisition

During the data acquisition, two main scanning parameters of TLS should be clarified, which are resolution and quality. These parameters affect the level of details captured during the scanning and thus need to be chosen based on the project requirements. Resolution determines the density of points, namely, distance between points. Quality in its turn, determines how long the scanner takes to measure a point and the length of time a point is sampled. Quality affects the rate of measurement and the level of noise reduction. The higher the quality, the less the noise will be, but time needed to capture each point will be higher. With the increasing resolution parameter, distance between scan points becomes less, while number of points enhance.

For the TLS FARO Focus 330 HDR, time needed for scanning based on the quality parameter and depended on resolution is shown on the figure 3.4. Distance between points and their numbers regarding to resolution parameter are given in the Table 3.2.

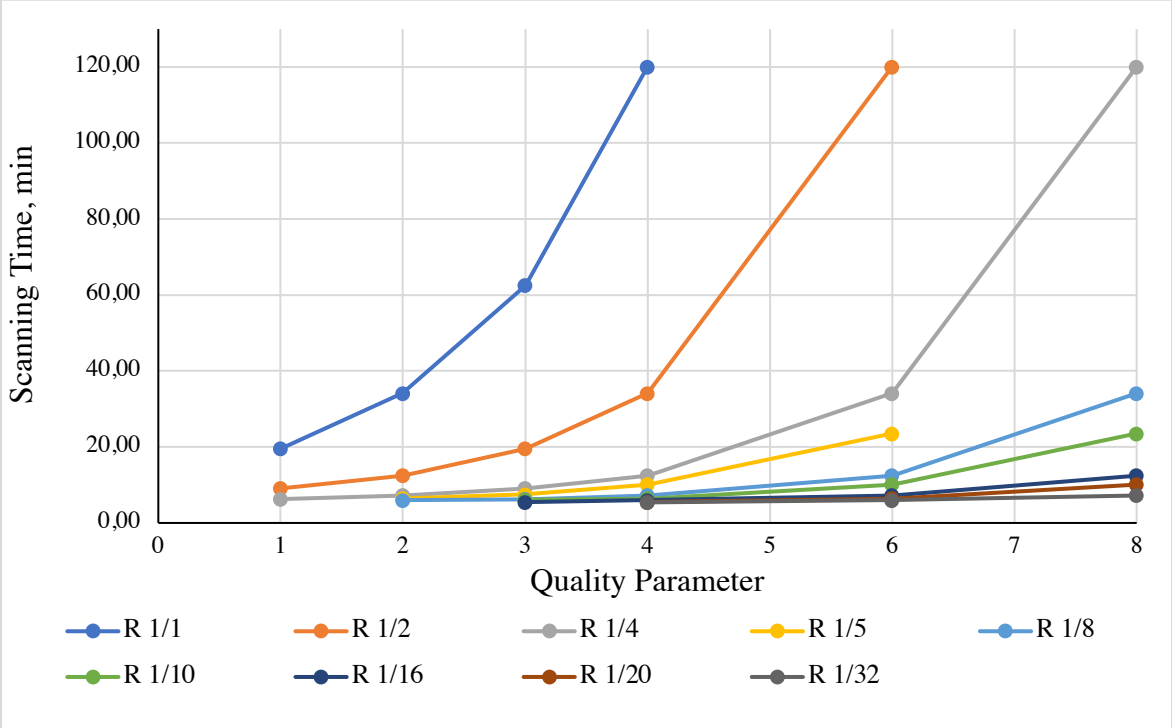

Figure 3.4. Scanning time based on the quality parameter.

Table 3.2. Point distance and numbers of points.

Resolution	1/1	1/2	1/4	1/5	1/8	1/10	1/16	1/20	1/32
Number of points, MPns	699.1	174.8	43.7	28.0	10.9	7.0	2.7	1.7	0.7
Point distance, mm	1.5	3.1	6.1	7.7	12.3	15.3	24.5	30.7	49.1

3.3. Processing of laser scanning data

3.3.1. Registration

When object is scanned, points are tracked and recorded in the Scanner Coordinate System (SCR). The origin (X; Y; Z) = (0; 0; 0) of this system is where laser meets mirror.

The number of these coordinate systems is equal to the number of TLS point stations. In order to determine the spatial relation between all these scans, registration process is needed. Thus, registration can be defined as a process of transforming all scans into the one coordinate system that is called Local Coordinate System (LCS). Georeferencing, in its turn, is the process of coordinate transformation from the LCS to the National Coordinate System (NCS). Workflow of these processes is shown on the Figure 3.5 and visualization of these coordinate systems is shown on the Figure 3.6.

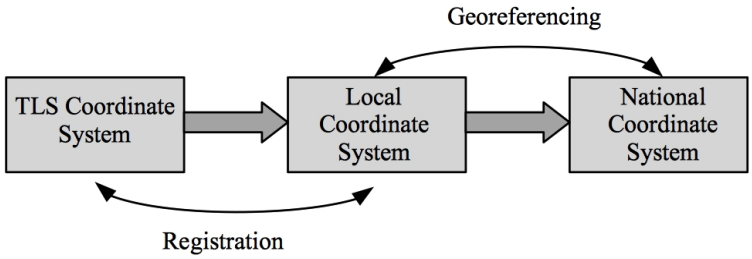

Figure 3.5. Workflow of coordinate transformation process.

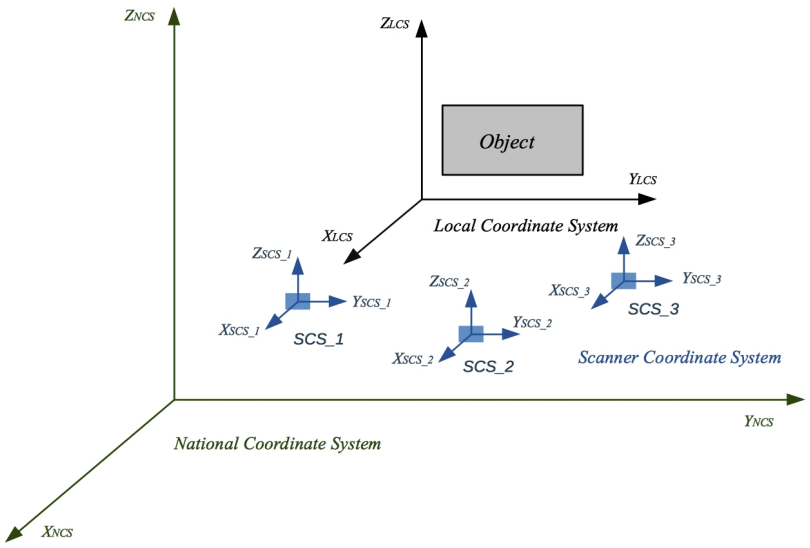

Figure 3.6. Types of coordinate systems: *SCS 1, 2, 3* – TLS' own Coordinate System related to its scan position; *LCS* – Local Coordinate System after the registration process; *NCS* – National Coordinate System after the georeferencing.

Registration process can be counted as the most important step in data processing. Errors in registration influence the quality of deliverables, whether this 3D mesh model or deviation maps in deformation analysis. It is important to choose the appropriate method of registration which will give the best accuracy and minimize the mean squared error between points after the registration (Goor, 2011). Registration can be performed using two most common methods, which are target-based and C2C.

The main principle of target-based method of registration relies on 3D coordinate transformation that transfers points from one 3D coordinate system to another (Chilani, 2017). In order to perform this transformation, seven parameters are needed which are:

- Three translations along the coordinate axes Tx, Ty, Tz, which are necessary to translate the origin of the first coordinate system to the second coordinate system;
- Three rotations around the coordinate axes Rx, Ry, Rz, which allow to rotate axes of the first coordinate system such they will coincides with the axes of the second coordinate system;
- Scale parameter which makes line lengths in the first coordinate system equal to their lengths in the second coordinate system.

Figure 3.7 shows the graphical representation of 3D coordinate transformation.

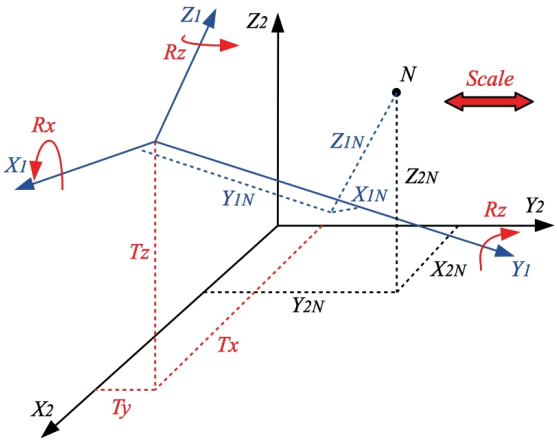

Figure 3.7. 3D coordinate transformation.

In order to determine these seven parameters, at least seven coordinates are needed over three points defined in both coordinate systems (Mataija *et al*., 2014). This is the main reason of making at least three targets common in each scan. In addition, these targets should have unique patterns, to be more precise, they should be widely spread not only in X and Y-directions, but also in Z-direction. The registration is then computed as the result of least square adjustment which minimizes errors. It is obvious that using more than three targets will improve the accuracy of transformation. Mathematical model of transformation can be written as:

$$V_T = \begin{bmatrix} X_T \\ Y_T \\ Z_T \end{bmatrix} = T + S_f . R . I = \begin{bmatrix} T_X \\ T_Y \\ T_Z \end{bmatrix} + S_f . \begin{bmatrix} R_X \\ R_Y \\ R_Z \end{bmatrix} . \begin{bmatrix} x \\ y \\ z \end{bmatrix} \tag{3.1}$$

where

V_T: transformed vector

T: translation vector

S_f: scale factor

R: rotation vector

I: initial vector

Rotation around the X-axis:

$$R_X = \begin{bmatrix} 1 & 0 & 0 \\ 0 & \cos\theta_X & \sin\theta_X \\ 0 & -\sin\theta_X & \cos\theta_X \end{bmatrix} \tag{3.2}$$

Rotation around the Y-axis:

$$R_Y = \begin{bmatrix} cos\theta_Y & 0 & -\sin\theta_Y \\ 0 & 1 & 0 \\ \sin\theta_Y & 0 & \cos\theta_Y \end{bmatrix} \tag{3.3}$$

Rotation around the Z-axis:

$$R_Z = \begin{bmatrix} \cos\theta_Z & \sin\theta_Z & 0 \\ -\sin\theta_Z & \cos\theta_Z & 0 \\ 0 & 0 & 1 \end{bmatrix} \tag{3.4}$$

The method of C2C registration has a principle of rigid transformation which maps one points set to the other without changing the distances between any two points in data set. Rigid transformation includes rotation and translation parameters (Yanik and Flores, 2009). In order to perform the transformation, the following steps should be realized:

- Finding the centroid of both data sets;
- Connecting the centroids of both data sets together;
- Implement rotation and translation to finish the transformation.

Mathematical model of the transformation can be represented as:

$$B_p = \begin{bmatrix} X^I \\ Y^I \\ Z^I \end{bmatrix} = R.A_p.T = \begin{bmatrix} R_X \\ R_Y \\ R_Z \end{bmatrix}.\begin{bmatrix} X \\ Y \\ Z \end{bmatrix}.\begin{bmatrix} T_X \\ T_Y \\ T_Z \end{bmatrix} \tag{3.5}$$

where

A*p*: {1, 2, 3} set of 3D point clouds

B*p*: $\{1^/, 2^/, 3^/\}$ set of 3D point clouds

R: rotation vector

T: translation vector

The most popular mathematical algorithm for C2C registration method is ICP. This algorithm was first introduced by Chen and Medioni (1992) and by Besl and McKay (1992). After, ICP algorithm was examined in greater depth by Zhang (1994), Rusinkiewicz and Levoy (2001), Low (2004), Pomerleau *et al*. (2015), and others. The main advantage of this algorithm is that it allows for iteration that is mathematical procedure implied in order to improve approximate solution (Du *et al*., 2010). Figure 3.8 shows the process rigid transformation of two point cloud sets $A = \{1,2,3\}$ and $B = \{1^I, 2^I, 3^I\}$.

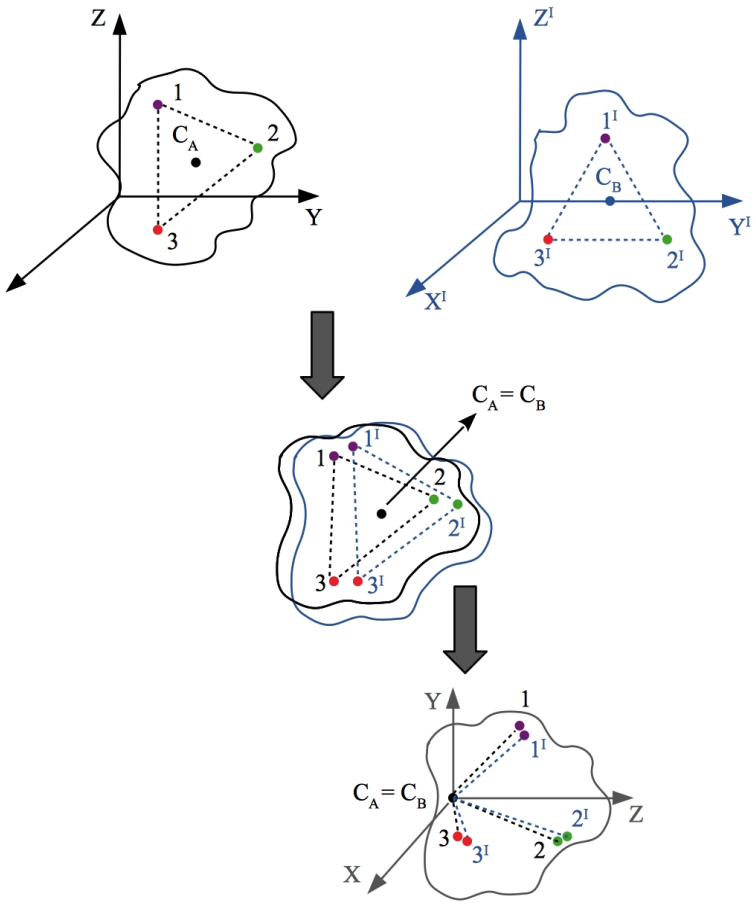

Figure 3.8. Workflow of rigid transformation.

3.3.2. Georeferencing

Once registration is finished, point cloud data may be aligned to the specific coordinate system NCS. This process is called georeferencing and can be done in two ways – direct and indirect, depending on the TLS design. Direct method can be applied if instrument has facilities like total station, to be more precise, TLS can be set up on the geodetic point with known coordinates. In this case, point clouds are obtained in NCS without performing any coordinate transformations. Indirect method implies using targets which coordinates have been computed before the scanning using total station observations for example (Abbas *et al.*, 2014). In this matter, TLS is not set up on the specific geodetic point and coordinate transformation, thus, may be performed using methods described in the Chapter 3.3.1.

Reshetyuk (2009) investigated direct and indirect methods of georeferencing on advantages and disadvantages. These results are shown in the Table 3.3.

Table 3.3. Comparing of direct and indirect methods of georeferencing.

	Direct method	**Indirect method**
Scan station	Scanning must be done from a special geodetic point with known (X, Y, Z) coordinates	Scanning can be performed from a random station or place
Overlapping	Overlapping is essential	There is no need in overlapping
Time needed for field operations	Point cloud data is georeferenced during the scanning, thus decreasing time of extra surveying	There is a need in extra geodetic surveying to compute (X, Y, Z) coordinates of targets
Post-processing	There is no need in post-processing in the office	Georeferencing is required a post-processing using special software
Accuracy of georeferencing	Lower accuracy	Higher accuracy

3.3.3. Point Cloud Filtering

During the data acquisition, some obstructions such as movement of people, cars, dust, or even the wind may become a reason for noise in data. A snapshot of noise in data set is shown in the Figure 3.9. These noisy points can be removed using filtering options, that are usually delivered by special software. For example, SCENE, that is a software manufactured by FARO company special for the TLS FARO, provides four types of filters:

1. Dark scan point filter;
2. Distance filter;
3. Stray point filter;
4. Edge artifact filter.

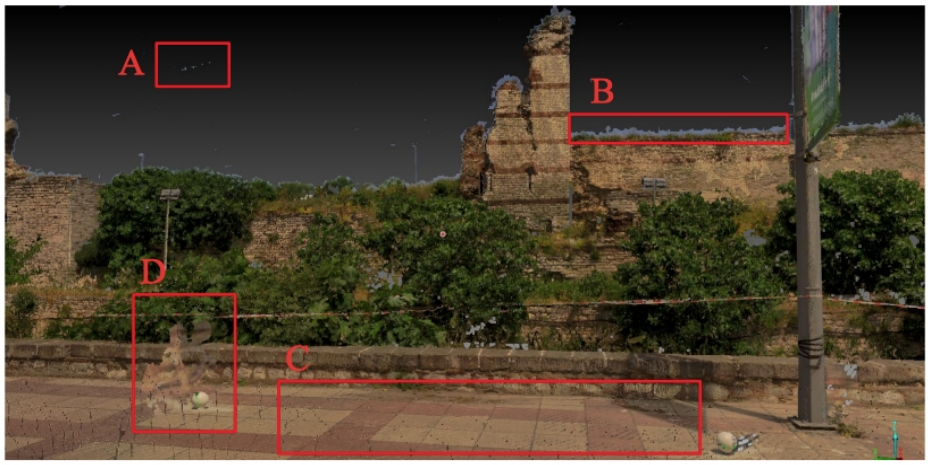

Figure 3.9. Noise in data set: (A) and (C) shows noise because of wind and dust in the air; (B) shows noise probably resulting from hitting the sky with the laser beam; (D) represents noise due to movement of people.

Dark scan point filter is usually used when scanning in black and white colors and is not applied on colorized scans. This filter eliminates points based on a reflectance value. When scanning in dark colors, only a small amount of light will be returned to the scanner, therefore the accuracy of points will be decreased. In this case, dark scan point filter is sufficient in use.

Distance filter deletes points outside the particular range, that is defined by setting the minimum and maximum distances from the scanner.

Stray point filter is used to remove outliers from the data set. The principle is based on the evaluation of points in the grid, which size is defined in settings. Stray point filter counts how many points in the grid have the same distance to the scanner, thus enabling to identify the outliers.

Edge artificial filter is useful to remove artifacts at the edges of objects. As it was mentioned in the Chapter 2.4.1.4, when laser meets edges of the objects, it can be spitted in two, thus resulting in false reflection. This filter works well during indoor scanning but may be competitive when scanning outdoors.

There is no strict order whether to apply filtering before or after the registration, however, this procedure must be done before starting the 3D modelling (Temizer *et al*., 2013). Otherwise, the expected outcomes will not have a good accuracy.

Sometimes, there is no need to use all the scanned points in data set. Project requirement may be smoothed to get only a certain part of the structure or building, as it is shown in the Figure 3.10. In this case, millions of unnecessary points can be completely removed from the data set by using special instruments (clipping box, for example) or manually. It usually takes several minutes to delete these extra points.



Figure 3.10. Point cloud project. Red rectangle represents the part of points that are needed for project deliverable.

3.3.4. Mesh modelling

Mesh model can be defined as a solid representation of the object in 2-dimentional (2D) or 3D dimensions from point cloud data. Mesh model consists of a set of triangles or quadrats in 2D and pyramids or hexahedrons in 3D, that are connected by their common corners. The process of meshing is schematically shown in Figure 3.11.

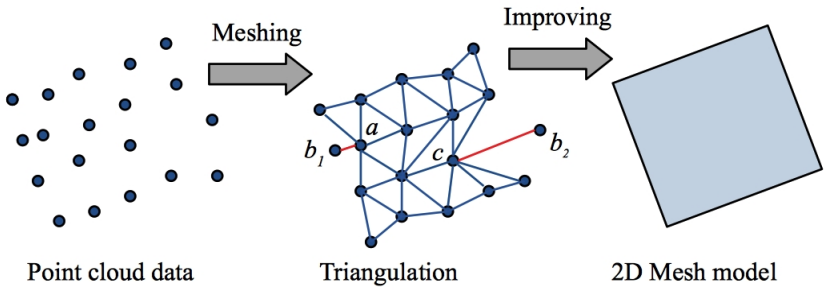

Figure 3.11. The process of 2D meshing by means of triangles.

Numbers of triangles can vary, obviously the larger the number of triangles, the more accurate will be the mesh model. The main criteria for choosing neighbor point are the angles and the distances of triangle's sides. These parameters can be defined manually in the software. As it can be seen from the Figure 3.11, because the distance between point *a* and b_1 is less and the distance between point *c* and b_2 is greater than the distance defined in the software settings, these points are not connected together. After the triangulation, mesh model can be improved by applying smoothing, hole filling and improving color.

Mesh models are widely used for building reconstruction and preservation purposes, as well as for the deformation analysis, where the point clouds from the 1. Epoch are converted into the mesh model, which in its turn is used as a reference frame in data comparing.

4. GENERAL INFORMATION ABOUT DEFORMATIONS

4.1. Definition and types of deformations

In engineering, deformation can be defined as the changes in size and shape of an object due to applied forces. These changes may occur either slowly or suddenly. The systematic measurements conducted in order to determine deformation is called deformation monitoring and the interpretation of those measurements has a name of deformation analysis (Moor, 1998).

All types of engineering structures and buildings are undergone deformations, which can be in two forms: elastic and plastic. Elastic deformation can be defined as a deformation that has a property to disappear after the removing of external force. Hence, this deformation is reversible and non-permanent. Plastic deformation, in its turn, is not reversible and results in changes of the shape, size or even place of the object and counted as a permanent (Dowling, 2012). The simple example of the elastic deformation is water dam. When water reservoir is full, the dam itself undergoes elastic deformation, and after the water gushing, the structure takes its previous form. The example of the plastic deformation can be landslides, subsidence and crustal deformations. Figure 4.1 illustrates the stress-strain curve showing elastic and plastic deformations.

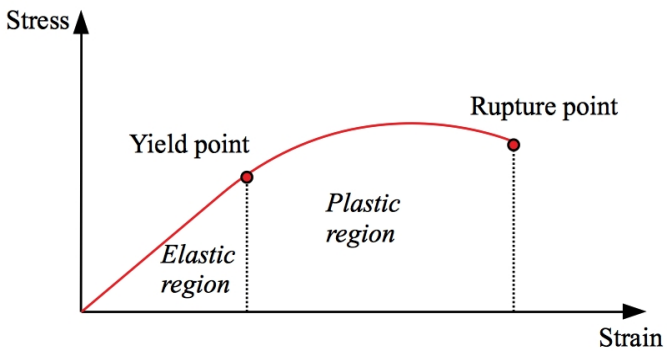

Figure 4.1. Stress-strain curve.

When object approaches the yield point, it is not able to turn into its original shape anymore and becomes a subject to permanent deformation. If applied forces continue to press the object, it may attain the rupture point, and in this moment fractures or cracks occur. There are five fundamental types of loadings on the object and they are shown in the Figure 4.2.

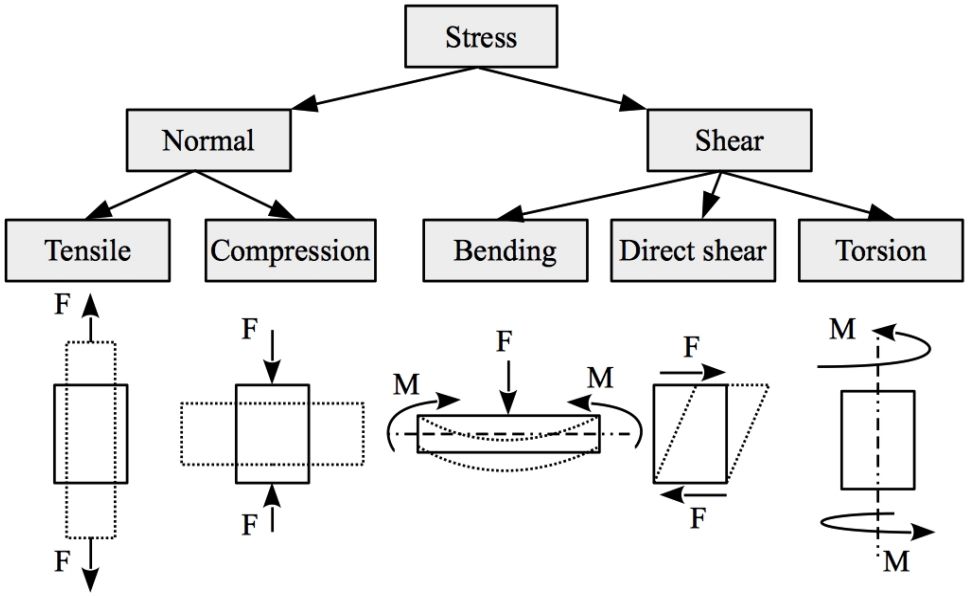

Figure 4.2. Types of stresses: F – force, linearly applied on the object; M – force that causes bogy to rotate.

In general terms, stress σ can be defined as force F applied on the object, divided by the object cross section's area A:

$$\sigma = \frac{F}{A} \tag{4.1}$$

Strain ε is the deformation of the object that results from an applied stress:

$$\varepsilon = \frac{L - L_0}{L_0} \tag{4.2}$$

where

L_o: original length of the object

L: length after the applied force

4.2. Reasons of deformations in historical structures

The main reasons of deformations in historical buildings can be divided into two groups – external and internal. The reasons related to the external group are associated with the forces that applied on the structure from outside, the reasons related to internal group, in its turn, are associated with reactions and changes that occur inside the structure (Thagunna, 2014). These reasons usually cause cracks on the structures and they are shown in the Figure 4.3.

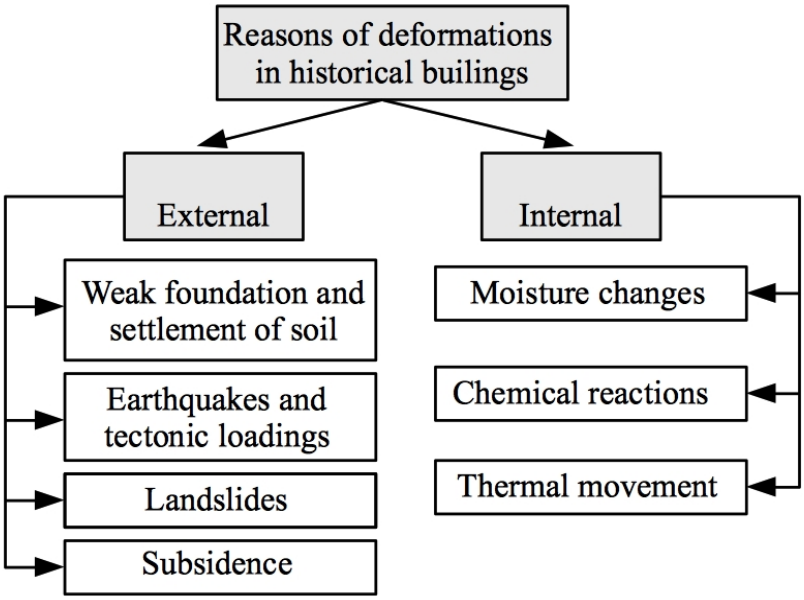

Figure 4.3. Reasons of deformations in historical buildings.

Since most historical buildings are made of ancient masonry which have been threatened by effects of decay, undergone tectonic loadings or settlements, it is not an unusual phenomenon to observe the cracks and the fractures on their walls. As mentioned by (Doshi *et al*., 2018), cracks can be classified according to their width and based on visual inspection. This classification is given in Table 4.1.

Table 4.1. Classification of cracks in masonry building (Doshi *et al*., 2018).

Degree of damage	Description	Crack width
Negligible	Hairline cracks	< 0,10 mm to 0,15 mm
Very slight	Fine cracks which can easily be treated during normal conservation	≈ 1 mm
Slight	Cracks which can be easily filled and probably require re-decoration. Possible need of reporting to ensure weather-tightness	< 5 mm
Moderate	Moderate cracks which can be easily patched or masked by suitable linings	5 – 15 mm
Severe	Large cracks which require extensive repair work. Impair of functionality	15 – 25 mm
Very severe	Very large cracks which require major repair job. Danger of instability	> 25 mm

4.3. Standards for deformation monitoring

Deformation monitoring requires a good practical and theoretical knowledge of deformation mechanism, needed for correct estimation and interpretation of deformation. According to USAGE (2002), there are some steps that must be taken into consideration before starting the deformation monitoring and they are shown in the Figure 4.4.

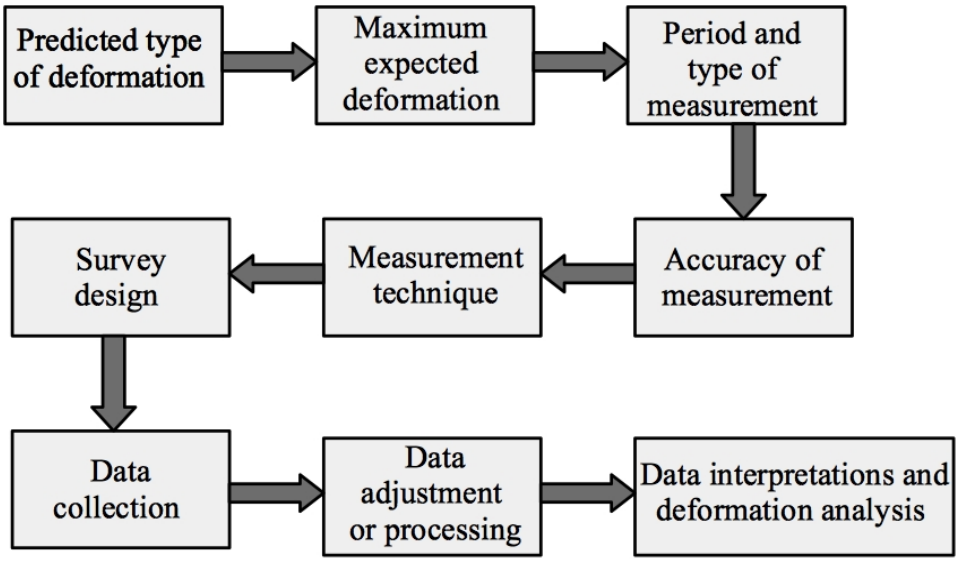

Figure 4.4. Workflow of deformation monitoring.

The time interval between the measurement periods is determined depending on the maximum expected value of deformation, and also based on factors that affect the structure (Kurt, 2010). Once the expected value and periods for surveying are determined, the accuracy can be discussed. Accuracy requirements mainly based on the maximum deformation value and can be calculated by the Formula 4.3.

$$Accuracy\ of\ measurement = \frac{1}{4}\ D_{max} \tag{4.3}$$

where

D_{max}: maximum deformation value

For example, it is known from the previous studies that the settlement of water embankment dam is approximately 50 mm per year, thus the required survey accuracy will be 12 mm (USAGE, 2002). Cracks usually require extending over months or even years before a valid assessment can be made (Jaafar, 2017). Hence, the period for monitoring structures with cracks or fractures can be specified to be from 6 to 12 months.

There are plenty number of techniques that are available for deformation measurements and they are shown in the Table 4.2.

Table 4.2. Geodetic techniques for deformation monitoring obtained from Kalkan *et al*. (2010) and Herban *et al*. (2014).

Type of technique	**Instruments**
Conventional survey	TS, Theodolite, Electronic Distance Measurement (EDM)
Precise Trigonometric Leveling	Precise Theodolite
Precise Geometric Leveling	Precise Leveling
Satellite based survey	GPS, GNSS
Interferometric Synthetic Aperture Radar (InSAR)	InSAR images processing
Digital close-range photogrammetry (DCRP)	Photogrammetric images processing
Laser Scanning technology	TLS, Mobile Laser Scanners

Survey design, data collection and data adjustment are based on the chosen survey technique. Deformation analysis is done based on coordinate difference and performed using statistical approaches (e.g., Gümüş, 2010). Figure 4.5 illustrates the deformation of cube-shaped object after some periods of time. Points are selected on the object and their coordinates are calculated from the geodetic measurements. After the certain period of time, the object changes its shape and size, and obviously, the position of points is also changed. Calculating the difference between the initial coordinates and coordinates obtained after the deformation, will give the value and the direction of displacement.

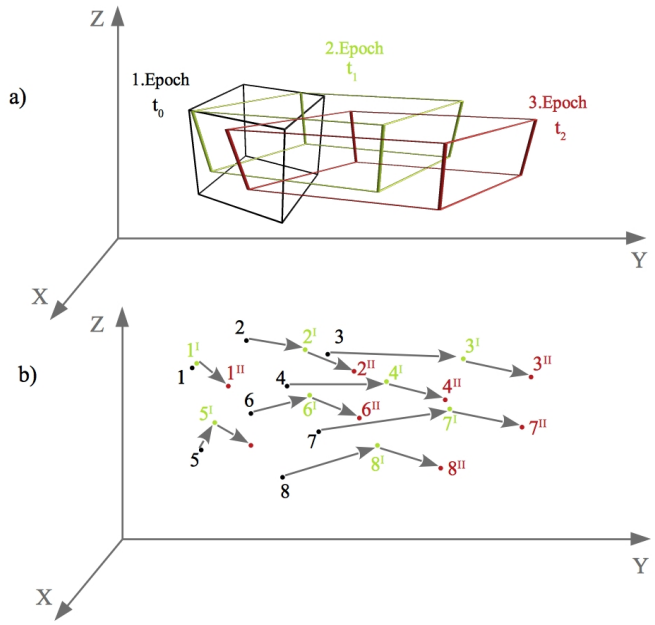

Figure 4.5. Determination of deformation: (a) Deformation of the object after the two time periods; (b) Determination of geodetic points coordinates and the vectors of deformation.

4.4. Methods of deformation analysis using Terrestrial Laser Scanning technology

4.4.1. Cloud-to-Cloud method

The main principle of C2C method consists of comparing two data set of point clouds and measuring the nearest neighbor distance between the reference and compared frames. Figure 4.6 shows the basic concept of C2C distance computation. This method was developed based on the Hausdorff distance (Oniga and Chirila, 2013), which can be defined as a maximum distance of a set to the nearest point in the other set (Jafari, 2016):

$$h(A_p, B_p) = max_{a \in A}\{min_{b \in B}\{d(a_A, b_B)\}\} \quad (4.4)$$

where

a_A: points of set Ap

b_B: points of set Bp

$d\ (a_A, b_B)$: Euclidean distance between a_A and b_B

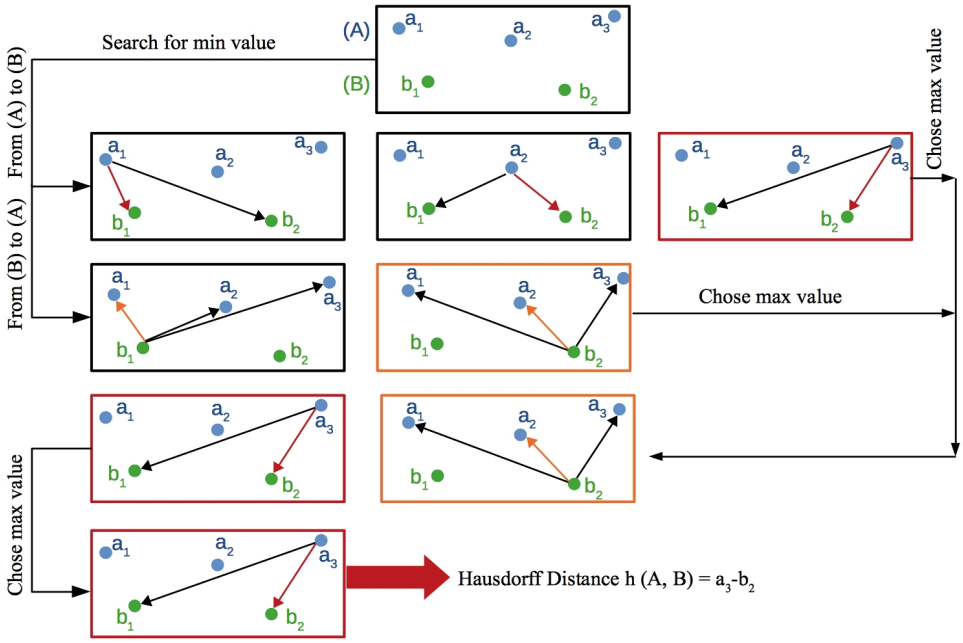

Figure 4.6. Basic concepts of C2C distance computation.

The value of deviation is calculated for each point of data set as a subtraction of reference coordinate from the measured in X, Y, and Z directions. The displacement vector, or 3D deviation, is calculated according to the formula (4.5):

$$DEV_{3D} = \pm\sqrt{\left(X_{meas} - X_{ref}\right)^2 + \left(Y_{meas} - Y_{ref}\right)^2 + \left(Z_{meas} - Z_{ref}\right)^2} \qquad (4.5)$$

where

X_{meas}, Y_{meas}, Z_{meas}: planar coordinates of the compared frame

X_{ref}, Y_{ref}, Z_{ref}: planar coordinates of the reference frame

The main advantage of this method is that it allows for very fast distance computation and does not require for distinguishing of points in the A and B sets (Figure 4.5). As for the disadvantages, point density usually varies for different scan positions and may lead to some uncertainties. However, as it was studied by Kersten *et al.* (2009), if to adhere to the same scanner settings and the same scanning geometry for all epochs, it will be possible to achieve even 0.5 mm of deformation accuracy (Tsakiri *et al.*, 2006).

4.4.2. Cloud-to-Mesh method

In C2M, deformation analysis is performed by comparing the second frame with the reference frame, which are given in the form of point clouds and mesh model respectively. Originally, reference frame is given in the form of point cloud, but the aim of C2M method is to create a mesh model from point cloud data that will represent the real surface of reference frame. Mesh model can be defined as representation of a surface in the form of triangular sets. Distance is calculated from each point in the compared frame to the nearest triangle in the reference frame. Figure 4.7 shows workflow of principle steps required in C2M method.

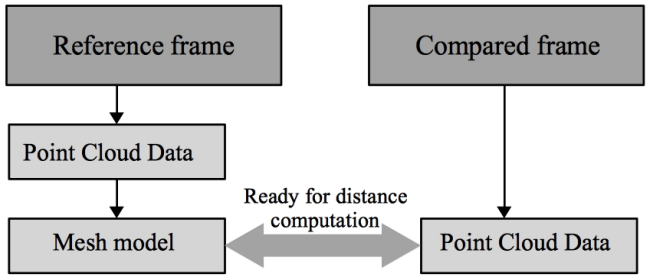

Figure 4.7. Workflow showing principle steps required in C2M method.

Several works were performed using this method of comparing (e.g., Gümüş, 2014; Ozdogan, 2019) and fairly good results were achieved. Although, Park and Lee (2019) found that point cloud approach was more stable in terms of accuracy than that of the mesh model. The main weakness of C2M method is that mesh model requires a dense point data. Low point density smoothers out some details that may be important (Lague *et al*., 2013).

4.4.3. Mesh-to-Mesh method

M2M method is similar to C2M with the only difference that compared frame is represented in the form of mesh model instead of point clouds. Figure 4.8 shows workflow of principle steps required in M2M method.

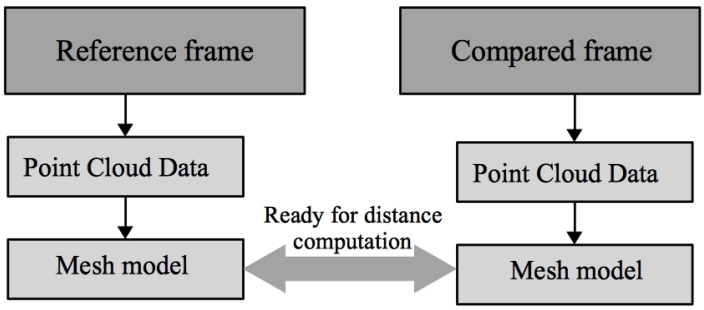

Figure 4.8. Workflow showing principle steps required in M2M method.

Generally, researches are tended to focus on the C2C or C2M methods rather than M2M, due to complexity of surface representation by means of triangles. The attempt to apply M2M method is shown by Lindenbergh and Pfeifer (2005) for deformation analysis of a lock. They divided the area of the lock into cells of 5×5 cm size and used all points in the cell to fit the plane. This method allowed to detect a deformation of 9 mm, but there is still considerable uncertainty with regard to the cell size. It is not clear if different cell size can give the same results or bring the difference in deformation value.

4.4.4. Error sources in deformation analysis

TLS technology has proven to be a good tool for the deformation monitoring of different structures due to possibility to acquire high resolution data quickly and accurately. However, despite such advantages, errors still cannot be eliminated. Based on the deformation analysis method discussed above, error sources in deformation analysis can be divided into three parts:

- Due to registration of point cloud data;
- Due to georeferencing of data;
- Due to unnecessary and uncleared points in data.

The final value of calculated distance can be thus represented by the Formula 4.6:

$$d_C = d_R + d_G + d_N \tag{4.6}$$

where

d_R: error after the registration

d_G: error after the georeferencing

d_N: error due to noise presence

Even if all errors cannot be completely removed from the data set, they can be significantly reduced. For example, the study of Gümüş (2008) has found that automatic method of registration gives better results compare to manual method. Yaman (2013) investigated the TLS position's accuracy according to the measurement distance and scanning angles. After the series of experiments, it was found that the most appropriate distance between the scanner position and the scanned object should be 40 – 50 m and the most accurate data were acquired from the laser station installed in front of the object, while data from the right and left stations showed the decrease in the amount of point clouds. According to Reshetyuk (2009), an efficient and appropriate approach for georeferencing is direct georeferencing, when the position of instrument is determined during the data acquisition. Also, as it is shown by Hepyörük (2015), georeferencing is not mandatory step in data processing. Deformation analysis can be performed using LCS after the registration. Another important thing that should be taken into account during the distance computation is the accuracy of 3D mesh model if such is used. The more points are obtained during the scanning, the better and more accurate the mesh model will be (e.g., Temizer *et al*., 2013). Furthermore, scanned structure must be filtered to get rid of extra points, otherwise, the deviation analysis will show a false result (Wei *et al*., 2010).

5. APPLICATION

5.1. Case study area

5.1.1. History of the case study area

The Walls of Istanbul is one of the most ancient and historically important structures of Istanbul that was controlled by the Roman, Byzantine, Latin and Ottoman Empires. It dates back to the year of 413 A.D., when the first construction began mainly for the defensive purposes. Designed by Anthemius and completed in 423 A.D., in the first year of the reign of Theodosius II, the Walls of Istanbul formed the border of Historical Peninsula that cover the area of almost 6 km^2. The Walls of Istanbul consisted of three parts: Land Walls, Sea Walls and Golden Horn Walls, the total length of which was around 22 km long (Turnbull, 2012). The Walls of Istanbul have been existed for 16 centuries, but unfortunately, a little part of it survived hitherto. Today, the Land Walls is a part of Historic Areas of Istanbul and since 1985 it has been added into the UNESCO World Heritage List. The historical map representing the Walls of Istanbul is shown in Figure 5.1.

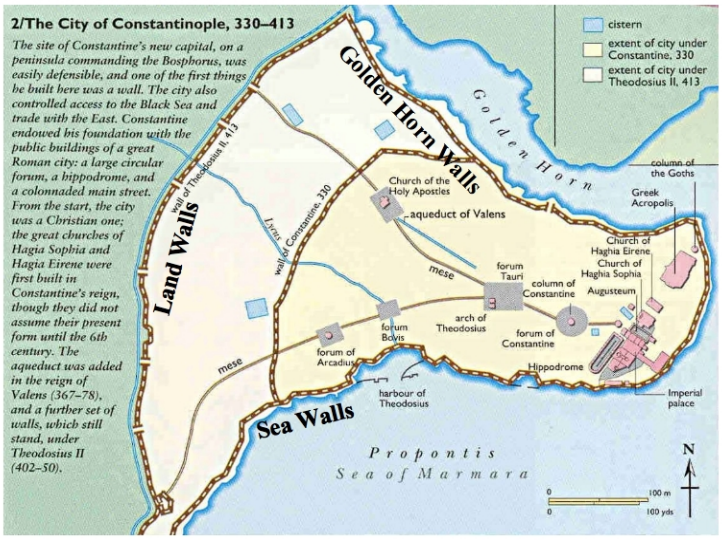

Figure 5.1. The map of Historical Peninsula showing Land Walls, Sea Walls and Golden Horn Walls (Turnbull, 2012).

Land Walls consisted of moat, low wall, outer wall, and inner wall. Moat was over 20 m wide and 10 m deep, was fenced with low wall and served as the first line of defense. Today, this area is used for the gardening purposes. the outer wall was built between the low and inner walls and was used as the second line of defense. This part was 2 m thick with the height of 9 m. the main and the most important part of Land Walls was the inner wall with 5 m thick and 12 m high. Both the outer and inner walls were strengthened with towers that were spaced at average distance of 40 – 60 m. only a little part of outer walls and their towers have survived till nowadays. The towers of inner wall have squared form with size 10 by 10 m and the height of 20 m and was made of limestone bricks. The construction scheme of Land Walls and their current state are shown in Figure 5.2.



(a) (b)

Figure 5.2. Land Walls of Istanbul: (a) Sections of the Land Walls after their construction (Turnbull, 2012); (b) Current state of Land Walls.

In this study, two towers of Land Walls that are examined on deformations, located approximately 1500 m apart each other. The coordinates of tower I are Latitude 40^0 59’ 51” and Longitude $28^0$55’ 17”. The coordinates of tower II are Latitude 41^0 00’ 40” and Longitude 28^0 52’ 22”. The location of towers on the map and their view are shown in Figure 5.3.

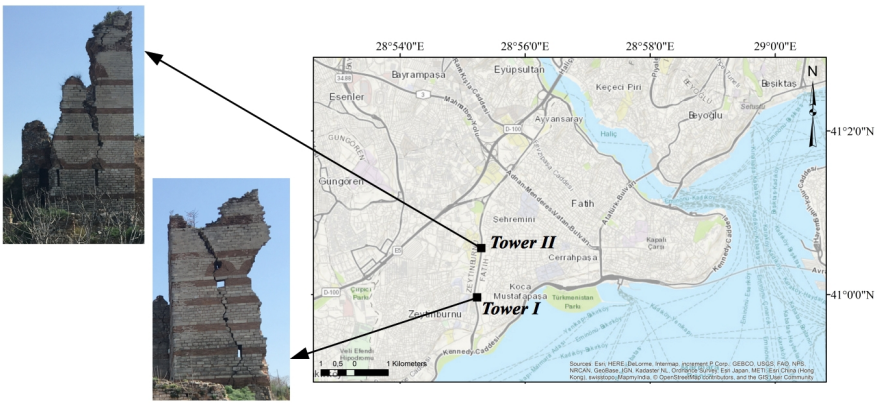

Figure 5.3. The case study area – location of towers on the map of Istanbul.

5.1.2. Seismicity of the case study area

Studied towers of Land Walls are situated very close to the Marmara Sea region, which seismicity is dominated by the right-lateral NAF. NAF is run from the eastern part of Turkey (41^0 E) to Istanbul in the west (29^0 E) with the length of approximately 1500 km and represents a plate boundary that separates Eurasian and Anatolian Plates at North and South respectively. This fault produced many earthquakes in the past, including those with the $M_w \geq 7.0$, and the Marmara region is counted as one of the most tectonically active areas in Turkey. Over the almost 1600 years, the Land Walls have been affected by many earthquakes and as many different studies show, the earthquake potential still cannot be ruled out (e.g., Once and Wilson 2006, Deniz and Ozener 2010, Ergintav *et al*. 2014, Ozener *et al.* 2018, Bulut *et al.* 2019). Among the biggest earthquakes that caused damage to the Land Walls, the following events can be considered: 447, 554, 740, 989, 1509, 1766, 1754, 1894, and 1999 (Ambraseys, 2002; Kalafat *et al*., 2007). After some of these earthquakes, Land Walls were such seriously destroyed that repair was impossible, and Walls were constructed again.

There are several earthquake catalogs that contain historical information about all events which took place in the Marmara region in the past (e.g., Ergin *et al*. 1967, Güçlü *et al.* 1986, Pınar and Lahn 1952, Soysal *et al*. 1981, Ambraseys and Jackson 2000, Kalafat *et al*. 2007).

Data are divided into two parts:

1. 400 – 1900 (historical period);
2. 1900 – till now (instrumental period).

The only drawback of the first period is that precise magnitude and coordinates of events cannot be derived exactly, but it still gives a good picture of underthrusting events in the past. For the period 400 – 1900, the most devastating events are given on the Figure 5.4 and for the period 1900 – 2019 are given on the Figure 5.5. Earthquakes with M_w<5.0 are not considered, as they can be counted as events with little hazard.

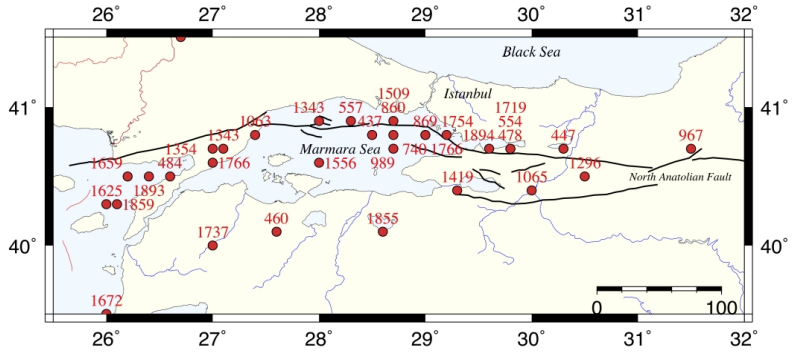

Figure 5.4. Historical earthquakes of Marmara region in the period of 400 – 1900 years given by Ambraseys (2002) and by Ambraseys and Jackson (2000).

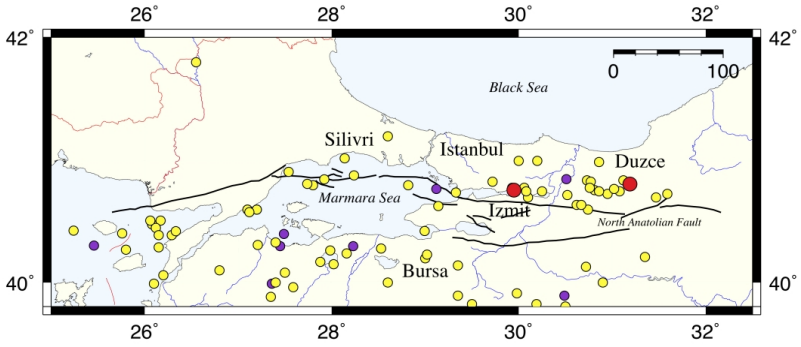

Figure 5.5. Historical earthquakes of Marmara region in the period of 1900 – 2019 years given by "KOERI-Regional Earthquake-Tsunami Monitoring Center" (KOERI, 2019); yellow color shows earthquakes with M_w 5 – 6; purple color shows earthquakes with M_w 6 – 7; red color shows earthquakes with $M_w \geq 7$.

Istanbul-Silivri earthquakes were occurred on September 24th and 26th 2019. According to "KOERI-Regional Earthquake-Tsunami Monitoring Center", on September 24, 2019 at 09:00 UTC (11:00 local time) the medium intensity earthquake (M_L 4.7, M_w 4.5) occurred in the Marmara Sea near Silivri town at the depth of 9.8 km. The coordinates of event are Latitude 40.8785 and Longitude 28.2090. Two days after, on September 26, 2019 at 11:59 UTC (13:59 local time) the medium intensity earthquake (M_L 5.8, M_w 5.7) occurred in the Marmara Sea close to previous event at the depth of 12.6 km. The coordinates of this earthquake are Latitude 40.8832 and Longitude 28.2110. Both earthquakes' epicenters were approximately 60 km from the Land Walls and according to the local newspapers, these two events had a destructive impact on the structure in some places. More than 150 aftershocks were recorded that continued throughout the month. Figure 5.6 shows the epicenters of these two earthquakes with aftershocks. Figures 5.4, 5.5 and 5.6 were drawn in Generic Mapping Tools software (Wessel *et al*., 2013). In addition, the North Anatolian Fault was given by Emre et al., 2011.

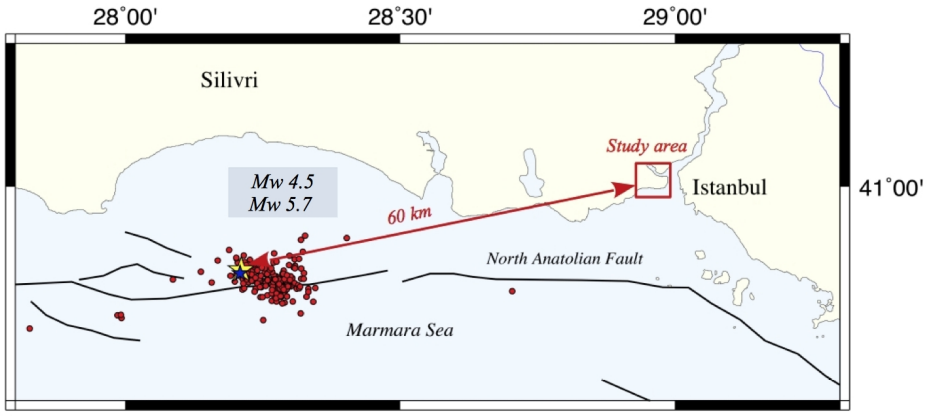

Figure 5.6. Istanbul-Silivri earthquakes and aftershocks: blue star – earthquake that occurred on 24th September 2019; yellow star – earthquake that occurred on 26th September 2019; red circles indicate aftershocks.

5.2. Terrestrial Laser Scanner used in application

In 1981, two engineers Simon Raab and Greg Fraser founded Res-Tech company, which name was changed after to FARO. In 2013, TLS FARO Focus 330 HDR was

introduced and quickly became a global leader in the manufacture of 3D measurement technology. Due to its professional benefits to capture all details quickly and accurate, TLS FARO Focus 330 HDR was chosen for application in the following thesis. Performance specifications of this instrument are shown in the Table 5.1 and its picture is represented in the Figure 5.7.



Figure 5.7. TLS FARO Focus 330 HDR (FARO Laser Scanner Focus 330 Manual, 2015).

Table 5.1. Performance specifications of FARO Focus 330 HDR (FARO Laser Scanner Focus 330 Manual, 2015).

Type	**Phase-based**
Scanning range	0.6 – 300 m indoor and outdoor scanning with upright incidence to a 90% reflective surface
Speed of measurement (pts/sec)	122,000/244,000/488,000/976,000
Ranging error	±2 mm
HDR	High Dynamic Range (HDR) photo recording
Parallax	Co-axial design
Field of view	Vertical 300^0 Horizontal 360^0
Laser class	Laser class 1

Wavelength	1550 nm
Beam divergence	Typical 0.19 mrad (0.011^0)
Beam diameter at exit	Typical 2.25 mm
Ambient temperature	5^0 – 40^0 C
Weight	5.2 kg

5.3. Process of work

5.3.1. Site documentation

Just before the process of scanning, the reconnaissance of study area was done. It was known that towers are located at the distance of 1500 m apart each other, thus, the process of scanning was decided to perform separately for each tower. The results of reconnaissance are given in Figure 5.8.

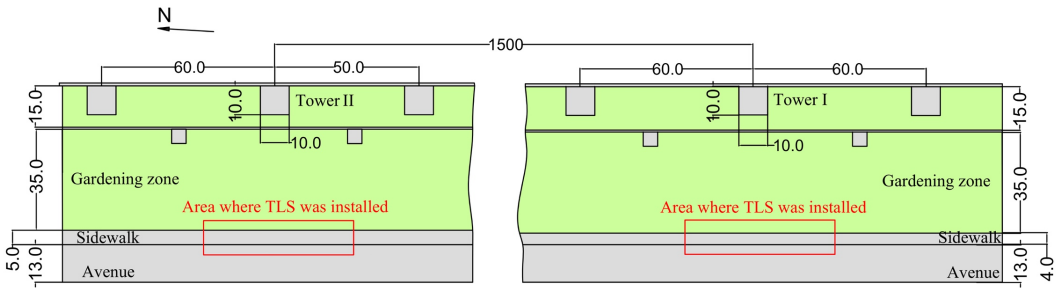

Figure 5.8. Results of reconnaissance (distances are shown in meters).

After the visual inspection of area near towers, it was revealed that several occlusions hindered the effective implementation of measurements. These are:

- There was not an opportunity to approach the structure as close as possible, because of the gardening zone in front of the Towers (Figure 5.9);
- There was a brick wall behind the each of the towers that made impossible to scan it from eastern side (Figure 5.10);

- Near the structure there was a dense vegetation that prevented to perform a single scan;
- Due to the fact that the structure has historical value, it was not allowed to place any objects on it, for example, checkerboards or markers.



(a) (b)

Figure 5.9. The surroundings of study area: (a) Tower I; (b) Tower II.



Figure 5.10. The surroundings of tower I from the East (taken from Google Earth).

Hence, taking into account all these obstacles, it was decided to perform scanning from several scan positions approximately 45 m from the structure. TLS was installed on the stable ground of sidewalk. It was decided to use spherical targets with the diameter of 145 mm which do not require a direct physical contact with the object. These targets were specially designed for FARO Focus 330 HDR and allow the highest possible scanning

efficiently from various directions due to excellent reflective properties. The set of spherical targets is shown in Figure 5.11.



Figure 5.11. Spherical targets.

5.3.2. Field operations

Towers were scanned three times with the 5-month period. Date of measurement campaigns are given in the Table 5.2. During the process of scanning, weather conditions were favorable enough, without rain, fog or snow.

Table 5.2. Date of data acquisitions.

	Tower I	**Tower II**
Epoch I	05.24.2019	06.18.2019
Epoch II	10.22.2019	11.07.2019
Epoch III	04.10.2010	04.10.2020

The scanning parameters such as resolution *R* and Quality *Q* were chosen to be R=1/1 and Q=1x for the first two epochs, and R=1/4 and Q=4x for the third epoch. The reason of it was the difficulties with data processing. During the first two epochs, scanning was

performed from three stand points for both Towers, while in the third epoch, TLS was set up 6 times. This was done because the resolution was decreased.

Six spherical targets were available for the use and during the process of scanning they were constantly moved such as three of them were common in each scan. This was done for the effective registration. Figure 5.12 shows the process of data acquisition.



(a) (b)

Figure 5.12. The process of scanning: (a) Tower I; (b) Tower II.

5.3.3. 3D point cloud processing

The processing of row data was performed in SCENE software (SCENE 2019.0 User Manual) that is the manufacturer software delivered with FARO Focus 330 HDR and was proceeded in three stages:

- Registration of scans taken from different stand points of TLS;
- Registration of epochs for further deformation analysis;
- Point cloud filtering.

The registration of scans tracked from TLS's stand points was done by target-based method of registration. Figure 5.13 illustrates the point cloud data before and after the

registration. Statistical results of target-based registration are presented in the Tables 5.3 and 5.4.

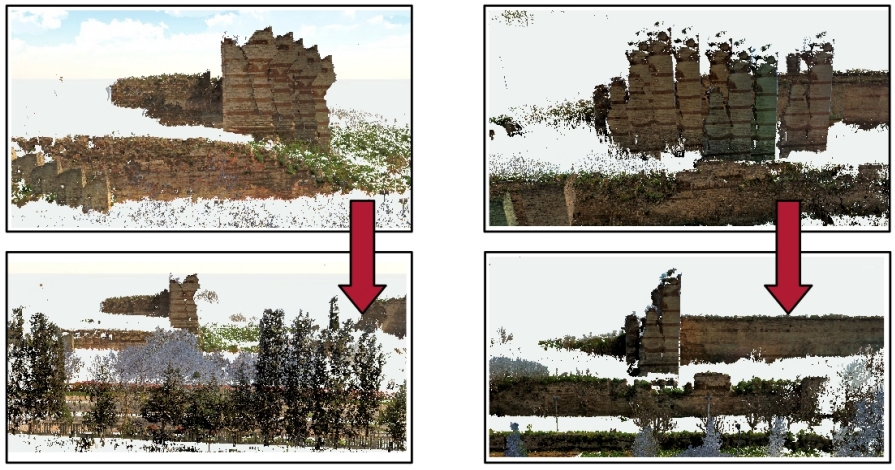

(a) (b)

Figure 5.13. Point cloud data before and after the target-based registration: (a) Tower I; (b) Tower II.

Table 5.3. Target statistics for the tower I.

	Epoch I 05.24.2019	**Epoch II 10.22.2019**	**Epoch III 04.10.2019**
Mean distance error, mm	0.8	2.9	2.2
Mean horizontal error, mm	0.8	0.5	1.4
Mean vertical error, mm	0.1	2.8	1.4

Table 5.4. Target statistics for the tower II.

	Epoch I 06.18.2019	**Epoch II 11.07.2019**	**Epoch III 04.10.2019**
Mean distance error, mm	2.1	2.0	2.6
Mean horizontal error, mm	1.1	1.0	1.5
Mean vertical error, mm	1.6	1.5	1.7

Once all scans are registered together, the registration of epochs can be done. This procedure was performed using C2C method of registration on account of the fact that spherical targets were not put at the same place during the scanning of epochs and thus, could not be used anymore. Figure 5.14 shows the epochs separately and their alignments after the registration. Statistical results of epochs' registration are shown in Table 5.5.

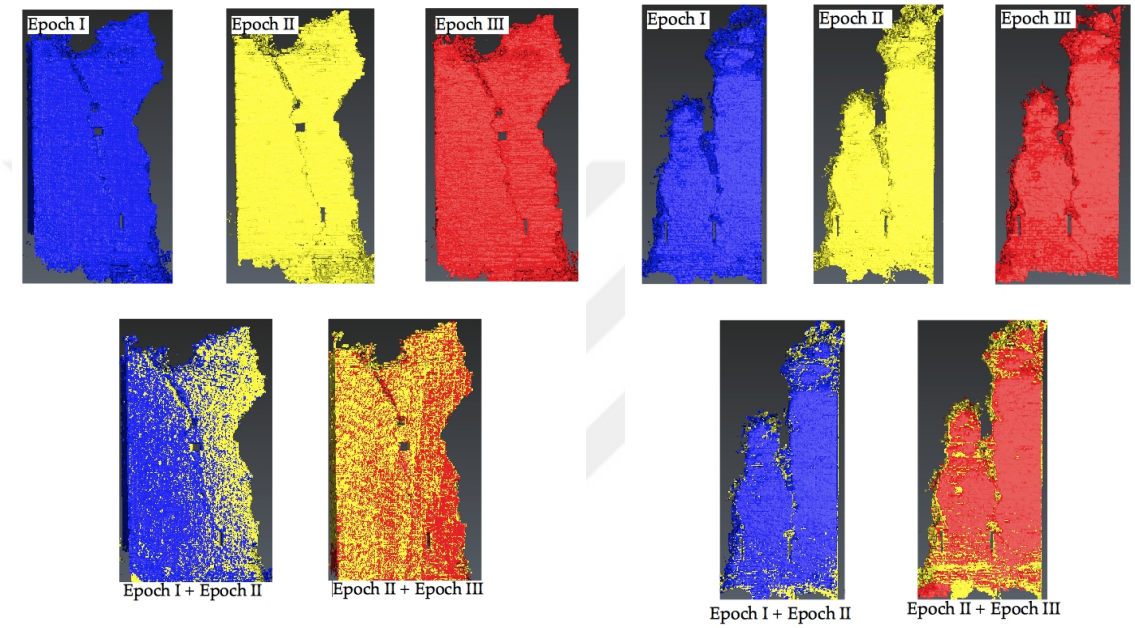

Figure 5.14. Single epochs and results of their registration: (a) Tower I; (b) Tower II.

Table 5.5. Scan statistics of epoch I, epoch II and epoch III.

	Tower I	**Tower II**
Maximum point error, mm	2.3	2.3
Mean point error, mm	1.3	1.2
Minimum overlap, %	56.5	65.2

As it can be seen from the Table 5.5, the alignment of all epochs resulted in overall error of 1.3 mm (for the tower I) and 1.2 mm (for the tower II), which means the average distance between two closest points. The registration errors are primary caused by

measurement errors, which can be reduced by fitting the appropriate scanning geometry. Another factor of errors is the point spacing between the data sets in overlap area. Reducing the distance between TLS' positions and increasing the density of point clouds may significantly lower the registration errors. In practice, the minimum mm errors of epochs' registration are of vital importance for deformation monitoring. In the current study, the obtained errors are relatively small and acceptable for the deformation monitoring of heritages.

The last step was point cloud filtering. Since the object of interest was only the front wall of the tower, there was no need to include all points in deformation analysis and all these extra points were removed. It was done by means of clipping box. Figure 5.15 illustrates the process of deleting points. After that, the part of tower was saved in E57 format and exported to the Cyclone 3DR software for further deformation analysis.

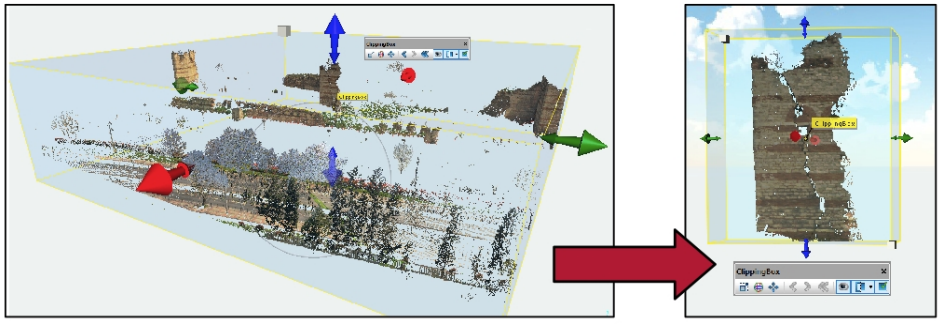

(a)

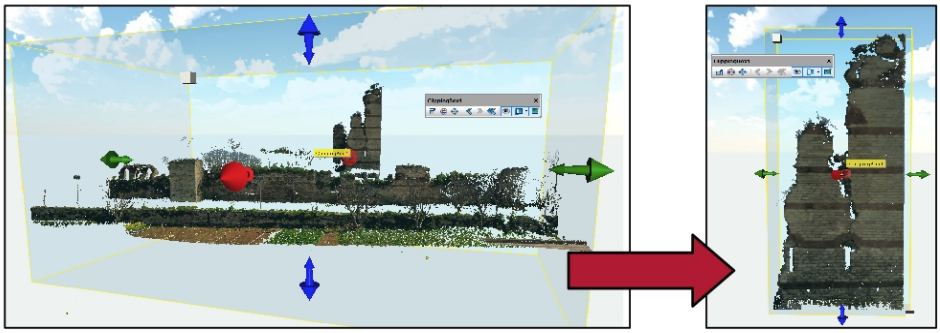

(b)

Figure 5.15. Process of point cloud filtering by means of clipping box: (a) Tower I; (b) Tower II.

5.4. Deformation analysis

Deformation analysis was performed using demo version of Cyclone 3DR software by C2C method of distance computation. The results of analysis for the first and second periods are given in the form of colored maps. The color scale represents the values of 3D displacements in meters. Grey patterns on the scale and on the map indicate areas that were not identified during the distance computation. The Z-axis represents a vertical direction. The Y-axis is oriented to the North and the X-axis is perpendicular to the Y-axis. All displacements have a positive value which means that the points of epoch II and epoch III are in front of those in the epoch I, which was selected as the reference frame.

5.4.1. Deformation analysis of tower I

The displacement map of tower I is given in Figure 5.16 and the percentage distribution of deviations is shown in Figure 5.17. The trend of the results illustrates that displacements occurred in the first period substantially higher in values, compared to the second period. Overall, the values ranged between 0 mm and 15 mm, with the average of 7 mm.

Figure 5.18 shows the distribution of displacements in sections A, B, C, and D. Displacements in highlighted sections in the first period are much higher compare to the displacements in the second period. Section A highlights its strong weathering susceptibility. It is unsurprisingly to find a considerable movement in the sections B and D due to huge cracks. Alternatively, it could simply mean that these parts of the structure undergo deformations independently of earthquake and therefore, it is reasonable to expect the continuation of displacements. In the section C, however, the obtained values of deviations are much lower in the second period compare to the first period. This may occurred due to construction weaknessess and section C can be construed as zone with potential risk of damage. It is obvious that another earthquake may destroy this corner.

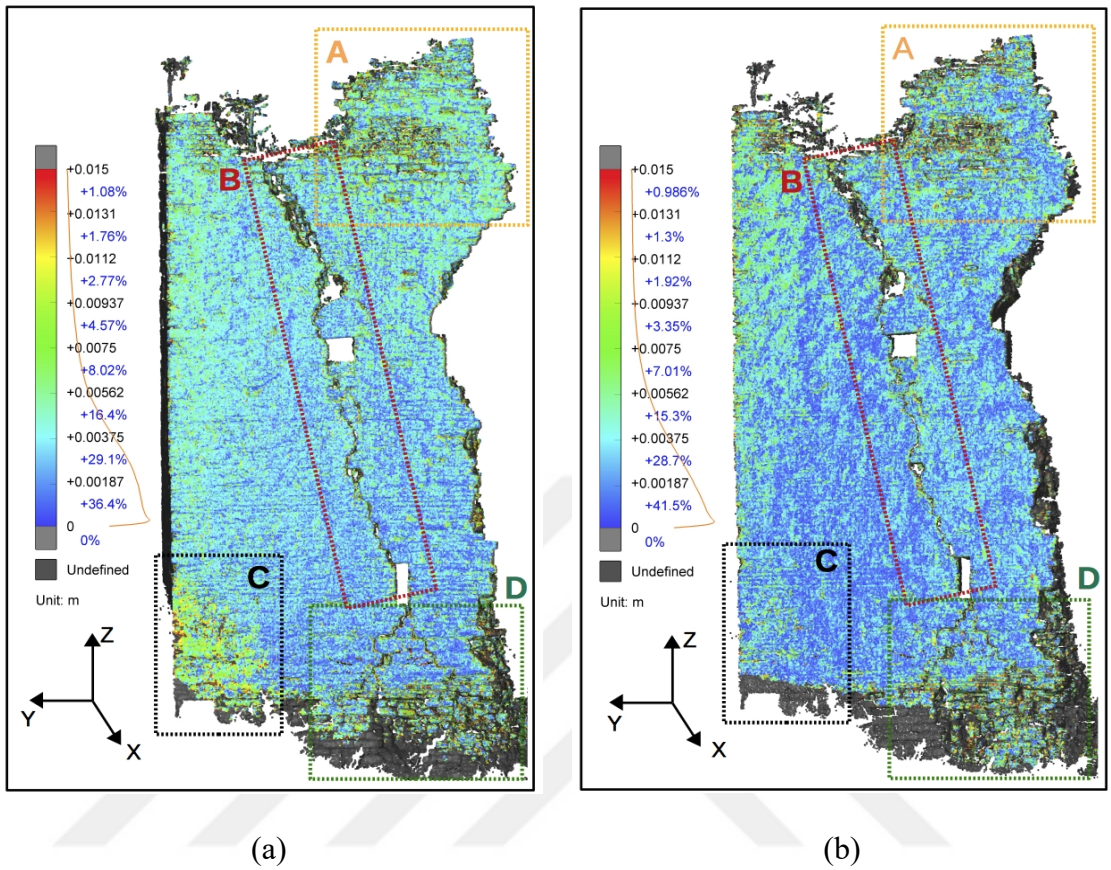

Figure 5.16. Deviation maps of tower I with areas of change highlighted (A, B, C, and D): (a) 1. Period comparing; (b) 2. Period comparing.

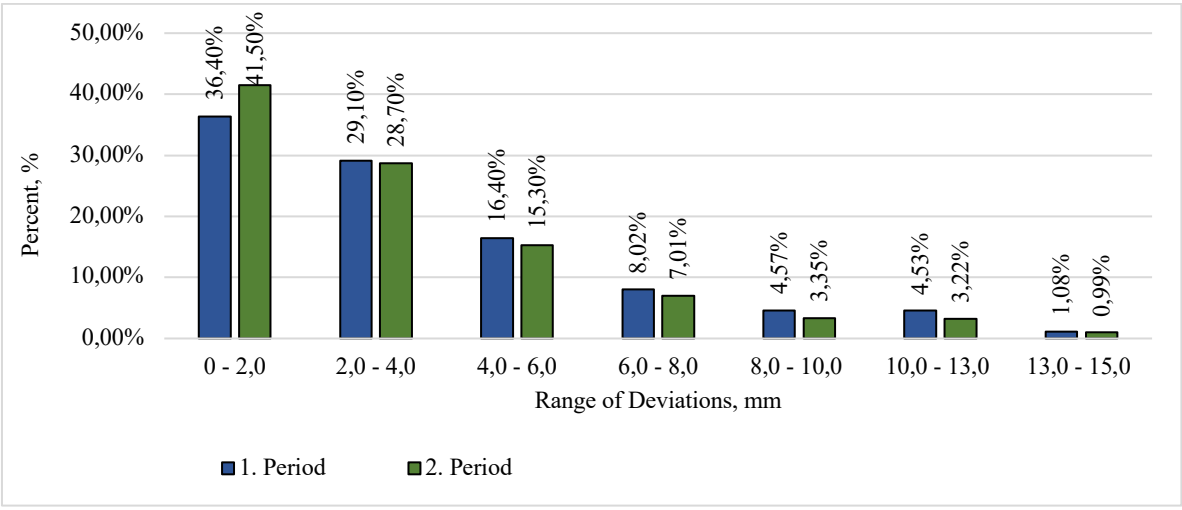

Figure 5.17. Percentage distribution of deviations in C2C analysis of tower I.

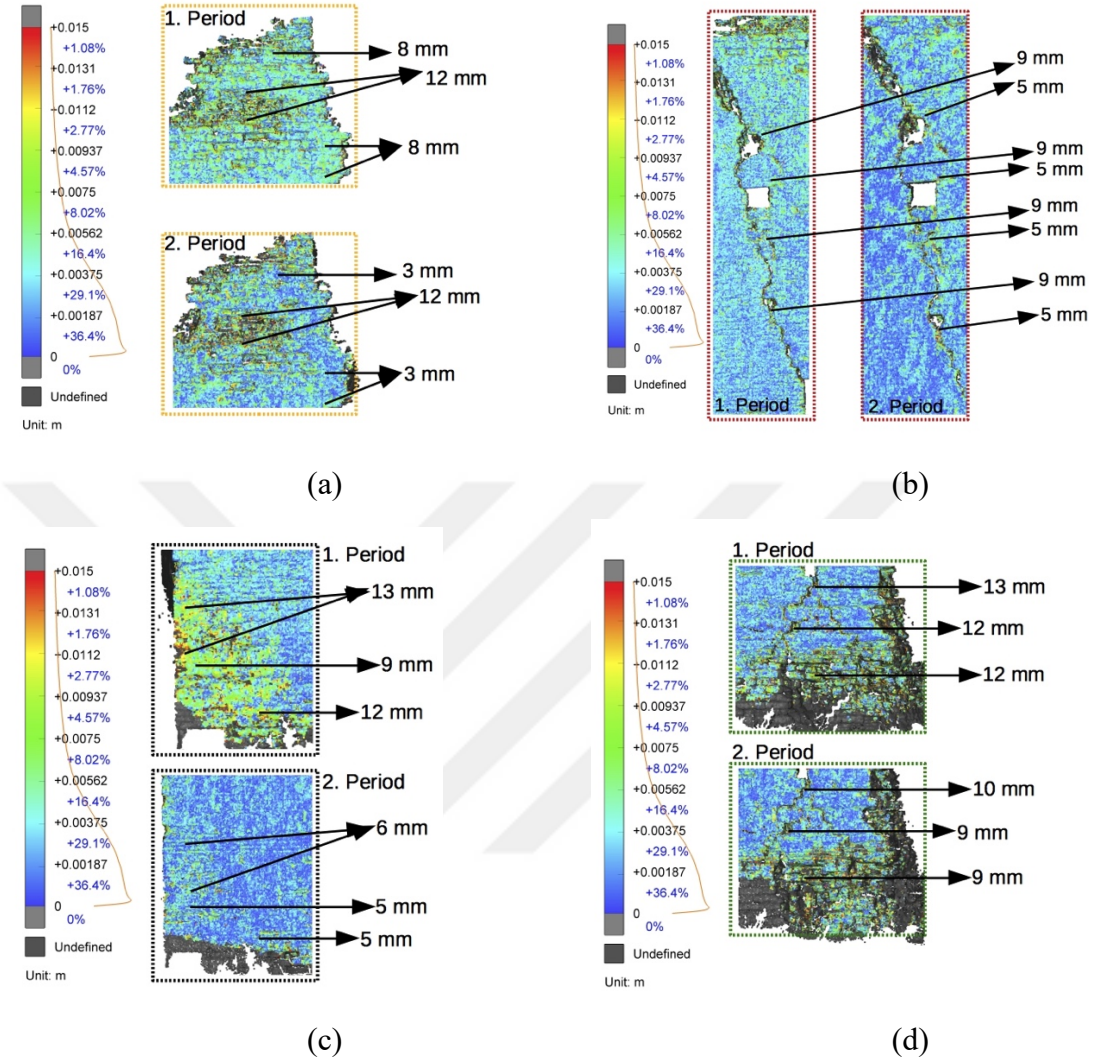

Figure 5.18. The distribution of displacements in the highlighted areas of tower I: (a) area A, (b) area B, (c) area C, and (d) area D.

5.4.2. Deformation analysis of tower II

The results of displacement computation of the tower II is given in Figure 5.19 and Figure 5.20 shows the percentage distribution of deviations.The range of displacements is changed from 0 mm to 20 mm. Considering this graph and the entire surface of tower II on the deviation map, it can be seen that almost all entire surface of the structure were exposed to displacements during the first period. While, in the second period, there are no remarkable displacements in general. This represents purely the effect of earthquake on the structure.

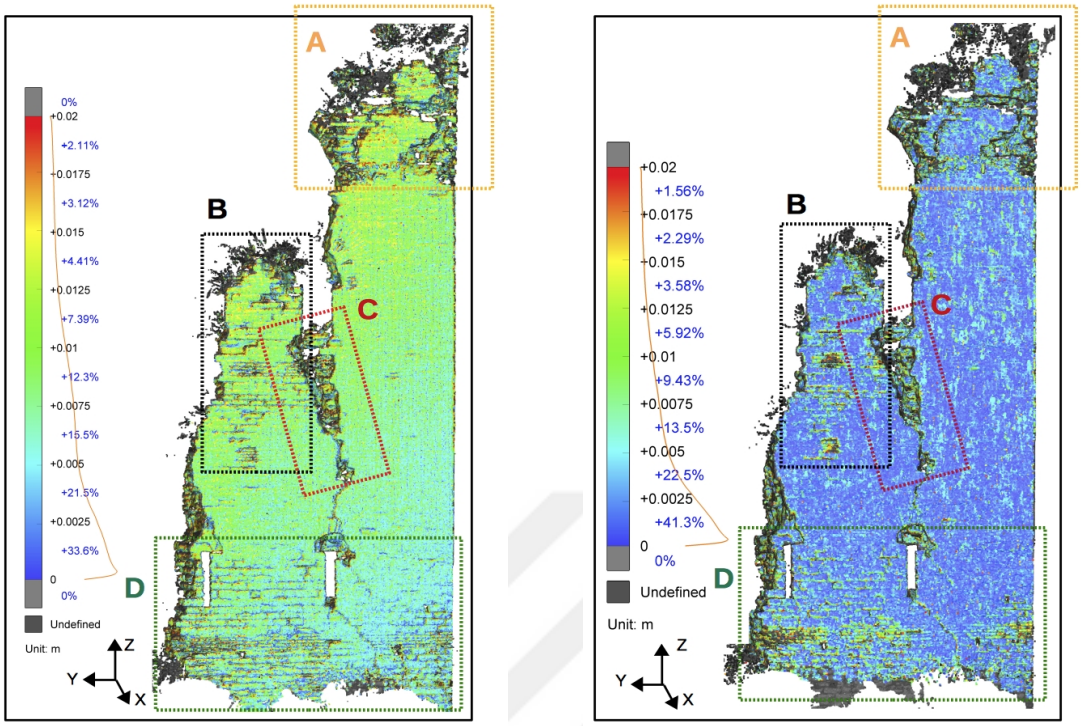

(a) (b)

Figure 5.19. Deviation maps of tower II with areas of change highlighted (A, B, C, and D): (a) 1. Period comparing; (b) 2. Period comparing.

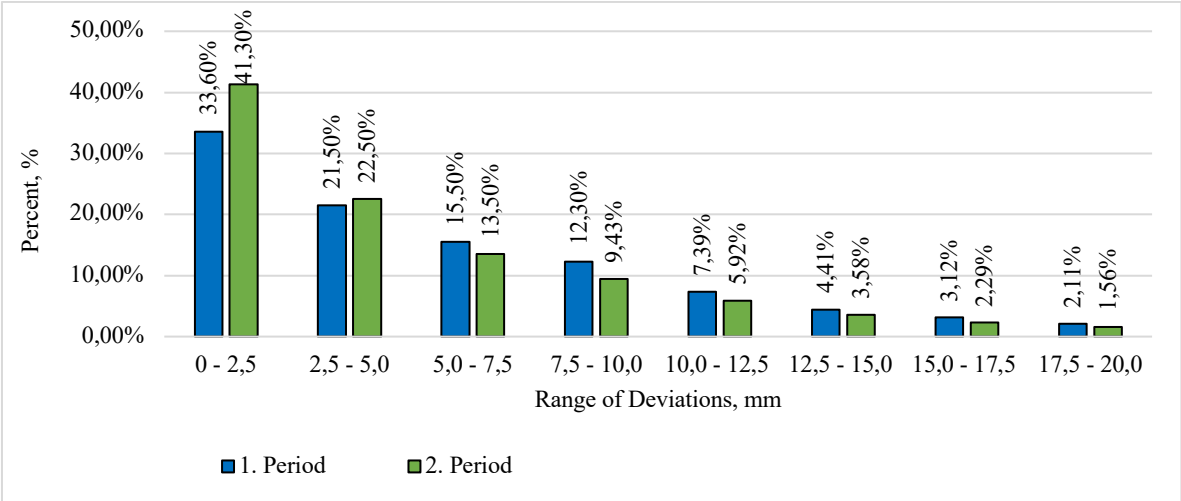

Figure 5.20. Percentage distribution of deviations in C2C analysis of tower II.

Figure 5.21 shows the distribution of displacements in sections A, B, C, and D. Sections A and B have great structural weaknesses and their positions been unstable. The discontinuities in bricks alignments in section D is been purely seen on the deviation maps.

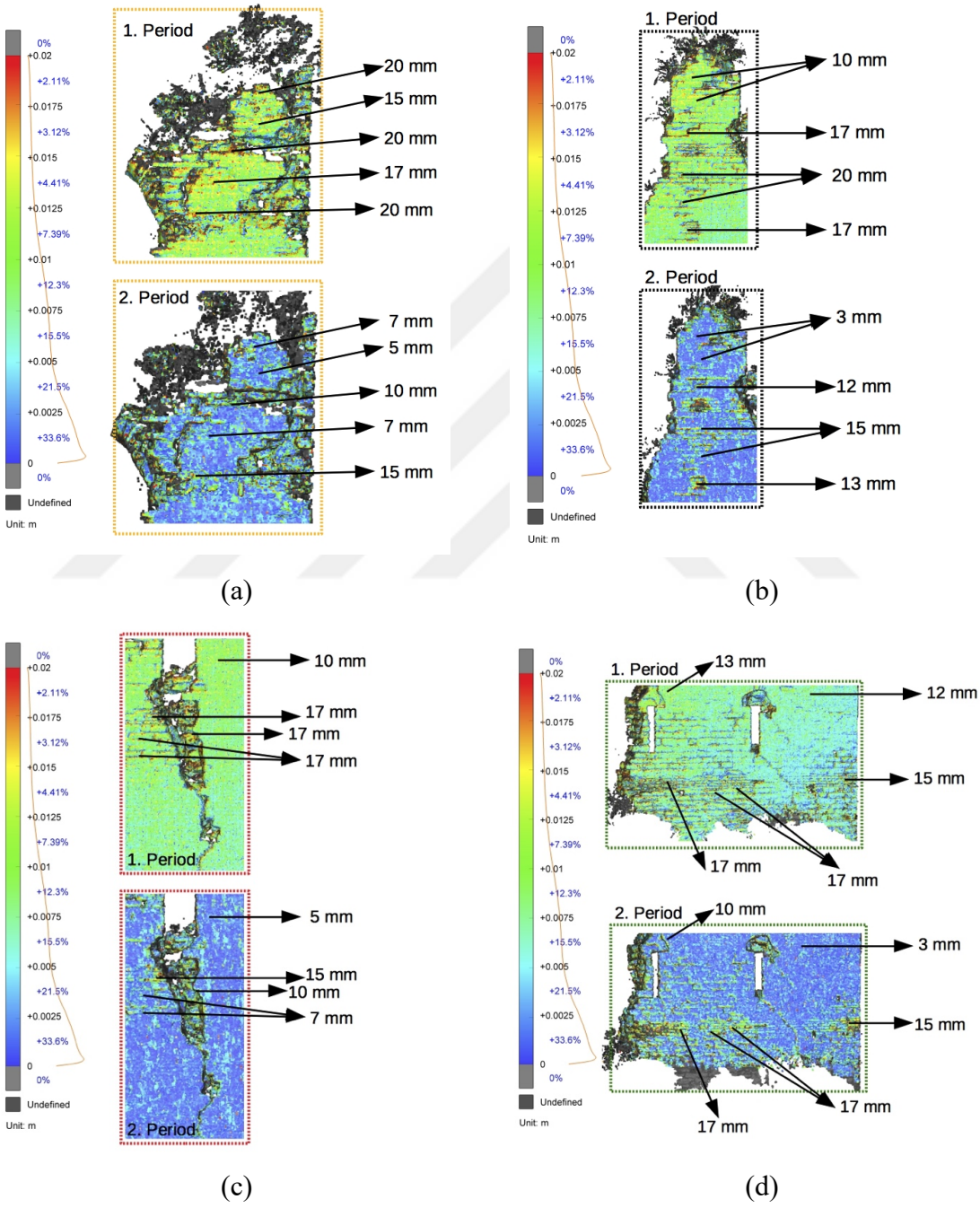

Figure 5.21. The distribution of displacements in the highlighted areas of tower II: (a) area A, (b) area B, (c) area C, and (d) area D.

6. CONCLUSIONS

TLS technology has been widely used in the deformation monitoring study in recent decades. Compare to other geodetic techniques, TLS makes it possible to acquire data in a very high level of accuracy and in the short period of time. Acquired data are given in the form of point cloud with X, Y, Z coordinates of each point respectively. Like all instruments, TLS is also prone to errors in measurements, but efforts are being made to improve the accuracy and minimize error sources.

In this application, it was of interest to perform the deformation analysis of two towers of the Land Walls of Istanbul due to huge cracks using TLS FARO Focus 330 HDR. In total, three measurement campaigns were done in the 5 months interval. A medium intensity earthquake with the magnitude of M_w 5.7 occurred between the first two campaigns of measurements and this event motivated to perform the third campaign in order to see if there was an impact of earthquake on the structures. After the visual inspection of studied area, the appropriate scanning geometry was organized. The scanning resolution 1/1 and quality 1x were chosen for the first two campaigns, however, due to unexpected difficulties with the data processing, these parameters were modified during the last campaign of measurements and new resolution was chosen as 1/4 and new quality as 4x. During the process of scanning the special spherical targets were used in order to register all separate scans together. Epochs were aligned with each other by C2C method of registration. These processes were done in SCENE software. Georeferencing was not performed and deformation analysis were done in LCS obtained after the registration of epochs. The mean distance errors after the target registration of all scans for the tower I were found to be 0.8 mm, 2.9 mm and 2.2 mm for the epoch I, epoch II and epoch III respectively. Alternatively, for the tower II, these values were 2.1 mm, 2.0 mm and 2.6 mm. The mean point errors of epochs' registration were 1.3 mm and 1.2 mm for the tower I and tower II respectively. The mean overlap in epochs' registration were 56.5% for the tower I and 65.2% for the tower II.

Deformation analysis was performed in Cyclone 3DR software using C2C method of distance computation. The results of deformation analysis are presented in the form of

colored maps. Returning to the hypothesis posed at the beginning of this thesis, it is now possible to state that the studied structures were affected by the earthquake that occurred approximately 60 km away with the magnitude of M_w 5.7. Hypothesis H_1 states that the values of deformations computed from the first and the second periods are not identical and if the deformations D_1 of the first period is greater than the deformations D_2 of the second period, it means that the deformations of the studied structure directly relevant to the earthquake. In the current case study, the Hypothesis H_1 is proven given that $D_1 > D_2$. To be more precise, the surface of tower I showed changes in the range from 5 mm to 15 mm in the first period and from 0 mm to 10 mm in the second period. The entire surface of tower II was exposed to deformations in the range from 7 mm to 15 mm in the first period, while in the second period the range was from 0 mm to 7 mm. The results of deformation analysis also helped to detect a zone of potential damage. To be more specific, the left lower corner of the tower I showed significant weaknesses in the first period, while in the second period of comparing there were no any serious changes.

As the future perspectives, the combination of different survey techniques and methods may improve this study by highlighting its strengths and weaknesses. For example, using TLS combined with GNSS may provide 3D point cloud data with geo-referencing in NCS. Another approach can be directed on the improvement of the 3D modelling by means of CRP, Unmanned Aerial Vehicle (UAV) or LIDAR. Terrestrial geodetic techniques such as TS should be additionally used in order to validate the obtained values of deformations. Additional work may be done on the registration analysis in order to exclude registration residuals from the discrepancies of the two clouds. The use of more than three spherical targets could make the assessment of the registration quality possible and measurement of some ground control points could help in control it. One of the ways to improve the methodology is to place spherical targets closer to the studied structures or to fix checkerboards directly on the walls of the structure after obtaining the approval of municipality.

All in all, TLS FARO Focus 330 HDR can be considered as a good tool for deformation monitoring purposes. The only drawback that can be pointed out is the huge data which require a lot of time to handle it. The C2C method of distance computation allows

to derive deformations within the mm accuracy and enable to indicate zones with potential risk of damage. However, the most attention must be directed at the registration processes as this influences the quality of deformation analysis.

REFERENCES

Abbas, M. A., Luh, L. C., Setan, H., Majid, Z., Chong, A. K., Aspuri, A., Ariff, M. F. M, 2014, "Terrestrial Laser Scanners Pre-processing: Registration and Georeferencing", *Jurnal Teknologi*, 71(4), pp. 115-122.

Abdelhafiz, A., 2009, *Integrating Digital Photogrammetry and Terrestrial Laser Scanning*, Master's Thesis, Technical University of Braunschweig.

Abellan, A., Vilaplana, J.M., Martinez, J., 2006, "Application of a Long-Range Terrestrial Laser Scanner to a Detailed Rockfall Study at Vall de Nuria (Eastern Pyrenees, Spain)", *Engineering Geology*, 88 (2006), pp. 136 – 148.

Alba, M., Fregonese, L., Prandi, F., Scaioni, M., Valgoi, P., 2006, "Structural Monitoring of a Large Dam by Terrestrial Laser Scanning", *International Archives of Photogrammetry, Remote Sensing and Spatial Information Sciences*, 36.5 (2006):6.

Ambraseys, N., 2002, "The Seismic Activity of the Marmara Sea Region Over the Last 2000 Years", *Bulletin of the Seismological Society of America*, *92*(1), pp. 1-18.

Ambraseys, N. N., Jackson, J. A., 2000, "Seismicity of the Sea of Marmara (Turkey) Since 1500", *Geophysical Journal International*, *141*(3), pp. F1-F6.

Antova, G., 2015, "Terrestrial Laser Scanning for Dam Deformation Monitoring – Case Study", *In FIG Working Week*, Sofia, Bulgaria (2015): 17-21.

Babic L., Dapo A., Pribicevic B., 2011, "Application of a 3D Terrestrial Laser Scanner in Industrial Applications on the Example of Objects on Gas Line "Slobodnica – Donji Miholjac", *In INGEO 2011 - 5th International Conference on Engineering Surveying*, Brijuni, Croatia, September 22-24, 2011.

Bajtala M., Bruncak P., Kubinec J., Liptak M., Sokol S., 2011, "Exploitation of Terrestrial Laser Scanning in Determining of Geometry of a Factory Chimney", *In INGEO 2011 - 5th International Conference on Engineering Surveying*, Brijuni, Croatia, September 22-24, 2011.

Bayram, B., Nemli, G., Ozkan, T., Oflaz, O.E., Kankotan, B., Cetin, I., 2015, "Comparison of Laser Scanning and Photogrammetry and their use for Digital Recording of Cultural Monument Case Study: Byzantine Land Walls - Istanbul", *ISPRS Annals of Photogrammetry, Remote Sensing and Spatial Information Sciences*, 2.

Besl, P. J., McKay, N. D., 1992, "Method for Registration of 3-D Shapes", *In Sensor fusion IV: control paradigms and data structures*, International Society for Optics and Photonics, Vol. 1611, pp. 586-606.

Bitelli, G., Dellapasqua, M., Girelli, V.A., 2017, "Historical Photogrammetry and Terrestrial Laser Scanning for the 3D Virtual Reconstruction of Destroyed Structures: a Case Study in Italy", *The International Archives of the Photogrammetry, Remote Sensing and Spatial Information Sciences*, Volume XLII-5/W1, 2017 Geomatics and Restoration – Conservation of Cultural Heritage in the Digital Era, 22–24 May 2017, Florence, Italy.

Boehler, W., Bordas Vicent, M., Marbs, A., 2003, "Investigating Laser Scanner Accuracy", *The International Archives of Photogrammetry, Remote Sensing and Spatial Information Sciences*, 34, pp. 696-701.

Bonali, E., Pesci, A., Casula, G, Boschi, E., 2014, "Deformation of Ancient Buildings Inferred by Terrestrial Laser Scanning Methodology: the Cantalovo Church Case Study (Northern Italy)", *Archaeometry*, 56.4 (2014): pp. 703 – 716.

Bulut, F., Aktug, B., Yaltirak, C., Dogru, A., Ozener, H., 2019, "Magnitude of Future Large Earthquakes Near Istanbul Quantified from 1500 Years of Historical Earthquakes, Present-day Microseismicity and GPS Slip Rates", *Tectonophysics*, 764, pp. 77-87.

Chen, Y., Medioni, G. G., 1992, "Object Modeling by Registration of Multiple Range Images", *Image Vision Comput*., 10(3), pp. 145-155.

Delaloye, D., Hutchinson, J., Diederichs, M., 2012, "Using Terrestrial Lidar for Tunnel Deformation Monitoring in Circular Tunnels and Shafts", *In Eurock 2012*, Stockholm.

Deniz, I., Ozener, H., 2010, "Estimation of Strain Accumulation of Densification Network in Northern Marmara Region, Turkey", *Natural Hazards and Earth System Sciences,* 10(10), 2135.

Doshi, M. S., Patel, D. B., Patel, K. B., Patel, K. B., Mavani, P. D., 2018, "Methodology for Prevention and Repair of Cracks in Building", *GRD Journals – Global Research and Development Journal for Engineering*, Volume 3, Issue 3.

Dowling, N. E., 2012, *Mechanical behavior of materials: engineering methods for deformation, fracture, and fatigue*, Pearson.

Du, S., Zheng, N., Ying, S., Liu, J., 2010, "Affine Iterative Closest Point Algorithm for Point Set Registration", *Pattern Recognition Letters*, 31(9), pp. 791-799.

Dursun, S., Sagir, D., Büyüksalih, G., Buhur, S., Kersten, T., Jacobsen, K., 2008, "3D City Modelling of Istanbul Historic Peninsula by Combination of Aerial Images and Terrestrial Laser Scanning Data", *In 4th EARSel Workshop on Remote Sensing for Developing Countries/GISDECO*, (Vol. 8, pp. 4-7).

Durusoy Ö. E., Can, M. C., 2018, "Conservation of the Land Walls Protection Area by Renewal (!): Evaluating the Spatial Effects of the Law No. 5366 Through "Zeytinburnu Culture Valley Project" of Istanbul", *Megaron*, 13(4).

Emre, O., Duman, T. Y., Ozalp, S., 2011, "1:250,000 Scale Active Fault Map Series of Turkey, Adapazari (NK 36-13) Quadrangle. Serial Number: 14", *General Directorate of Mineral Research and Exploration*, Ankara-Turkey.

Emre, O., Duman, T. Y., Ozalp, S., 2011, "1:250,000 Scale Active Fault Map Series of Turkey, Bursa (NK 35-12) Quadrangle. Serial Number: 9", *General Directorate of Mineral Research and Exploration*, Ankara-Turkey.

Emre, O., Duman, T. Y., Ozalp, S., "2011, 1:250,000 Scale Active Fault Map Series of Turkey, Bandirma (NK 35-11b) Quadrangle. Serial Number: 3", *General Directorate of Mineral Research and Exploration*, Ankara-Turkey.

Ercan, T., 2017, *The Use of Laser Scanning in Civil and Earthquake Engineering*, Master's Thesis, Boğaziçi University.

Ergin, K., Güçlü, U., Uz, Z., 1967, "A catalog of Earthquakes for Turkey and Surrounding area (11 A.D. to 1964 A.D.)", *Technical Report*, Istanbul Technical University, Faculty of Mines, Institute of Physics of the Earth, no. 24.

Ergintav, S., Reilinger, R. E., Çakmak, R., Floyd, M., Cakir, Z., Doğan, U., Özener, H., 2014, "Istanbul's Earthquake Hot Spots: Geodetic Constraints on Strain Accumulation Along Faults in the Marmara Seismic Gap", *Geophysical Research Letters*, *41*(16), pp. 5783-5788.

FARO Laser Scanner Focus 330 Manual, February 2015 Edition, © FARO Technologies Inc., 2015.

Georgopoulos, G. D., Telioni, E. C., Tsontzou, A., 2016, "The Contribution of Laser Scanning Technology in the Estimation of Ancient Greek Monuments' Deformations", *Survey review*, 48.349 (2016): pp. 303-308.

Ghilani, C. D., 2017, *Adjustment Computations: Spatial Data Analysis*, John Wiley and Sons.

Güçlü, U., Altınbaş, G., Eyidoğan, H., 1986, "A Catalog of Earthquakes of Turkey and Surrounding Area (1971 – 1975)", *Technical Report*, Istanbul Technical University, Faculty of Mines, no. 30.

Gümüş, K., 2008, *Yersel Lazer Tarayıcılar ve Konum Doğruluklarının Araştırılması*, Yüksek Lisans Tezi, Yıldız Teknik Üniversitesi.

Gümüş, K., 2014, *Yersel Lazer Tarayıcıların Doğruluk Araştırması ve Mühendislik Yapılarında Kullanılabilirliği: Oymapınar Barajı Örneği*, Doktora Tezi, Yıldız Teknik Üniversitesi.

Gümüş, M., 2010, *Yersel lazer tarayıcıların deformasyon ölçmelerinde kullanılabilirliği üzerine bir çalışma*, Doktora Tezi, Selçuk Üniversitesi.

Han, J. Y., Guo, J., Jiang, Y. S., 2013, "Monitoring Tunnel Deformations by Means of Multi-Epoch Dispersed 3D LIDAR Point Clouds: an Improved Approach", *Tunneling and Underground Space Technology*, 38: pp. 385-389.

Hendriatiningsih, S., Suwardhi, D., Januragadi, 2015, "3D Model Based on Terrestrial Laser Scanning (TLS) Case Study: The Cangkuang Temple, Garut District, West Java, Indonesia", *J. Eng. Technol. Sci*., Vol. 47, No. 1, 2015, pp. 1 – 19.

Hepyörük, G., 2015, *Tarihi ve Kültürel Varlıkların Belgelendirilmesi ve Üç Boyutlu Modelinin Oluşturulmasında Yersel Lazer Tarayıcıların Kullanım Olanaklarının Araştırılması ve Karacabey Türbesi (Ankara) Örneği*, Doktora Tezi, Selçuk Üniversitesi.

Herban, S., Grecea, C., Rusu, G., Alionescu, A., 2014, "Evaluation of Structure Deformation Using Geodetic Methods", *In 2nd European Conference of Geodesy and Geomatics Engineering*, (GENG, 14) Advances in Environmental Development, Geomatics Engineering and Tourism, pp. 157-162.

Ince, G. Ç., 2012, "Probabilistic Seismic Hazard Assessment of the Historical Peninsula of Istanbul", *Natural Hazards and Earth System Sciences*, 12(11).

Ince, G. C., Yildirim, M., Özaydin, K., Özener, P. T., 2008, "Seismic Microzonation of the Historic Peninsula of Istanbul", *Bulletin of Engineering Geology and the Environment*, 67(1), pp. 41-51.

Jaafar, H. A., 2017, *Detection and Localization of Structural Deformations Using Terrestrial Laser Scanning and Generalized Procrustes Analysis*, Doctoral dissertation, University of Nottingham.

Jaselskis, E.J., Gao, Z., Walters, R.C., 2005, "Improving Transportation Projects Using Laser Scanning", *Journal of Construction Engineering and Management*, Vol. 131, No.3, March 1, 2005, DOI: 10.1061/(ASCE)0733-9364(2005)131:3(377).

Kajzar, V., Kukutsch, R., Waclawik, P., Nemcik, J., 2017, "Innovative Approach to Monitoring Coal Pillar Deformation and Roof Movement Using 3D Laser Technology", *Symposium of the International Society for Rock Mechanics*, Procedia Engineering 191 (2017), pp. 873 – 879.

Kalafat, D., Güneş, Y., Kara, M., Deniz, P., Kekovalı, K., Kuleli, S., Özel, N., 2007, *Bütünleştirilmiş Homojen Türkiye Deprem Kataloğu (1900-2005; M≥ 4.0)*, Boğaziçi Üniversitesi Yayınları.

Kalkan, Y., Alkan, R. M., Bilgi, S., 2010, "Deformation Monitoring Studies at Atatürk Dam", *In FIG Congress: Facing the Challenges – Building the Capacity*, Sydney, Australia.

Kaloop, M. R., Beshr, A. A., Elshiekh, M. Y., 2008, "Using Total Station for Monitoring the Deformation of High Strength Concrete Beams", *In 6th International Conference on Vibration Engineering*, (ICVE'2008), Dalian, pp. 411-419.

Kanashin, N.V., Nikitchin, A.A., Svintsov, E.S., 2017, "Application of Laser Scanning Technology in Geotechnical Works on Reconstruction of Draw Spans of the Palace Bridge in Saint Petersburg", *In Transportation Geotechnics and Geoecology*, TGG 2017, 17-19 May 2017, Saint Petersburg, Russia.

Karabacak, V., Altunel, E., Cakir, Z., 2011, "Monitoring Aseismic Surface Creep Along the North Anatolian Fault (Turkey) using Ground-Based LIDAR", *Earth and Planetary science Letters,* 304 (2011), pp. 64 – 70.

Kayen, R., Collins, B.D., Bawden, G., Pack, R.T., 2006, "Earthquake Deformation Analysis Using Terrestrial Scanning Laser-Lidar Technology", *In Proceedings of the 8th U.S. National Conference on Earthquake Engineering*, April 18-22, 2006, San Francisco, California, USA, paper no. 1587.

Kersten, T. P., BüyüksalİH, G., Baz, İ., Jacobsen, K., 2009, "Documentation of Istanbul Historic Peninsula by Kinematic Terrestrial Laser Scanning", *The Photogrammetric Record*, 24(126), pp. 122-138.

Kersten, T. P., Mechelke, K., Lindstaedt, M., Sternberg, H., 2009, "Methods for Geometric Accuracy Investigations of Terrestrial Laser Scanning Systems", *Photogrammetrie-Fernerkundung-Geoinformation*, 2009(4), pp. 301-315.

Kırlangıç, A. S., Kesti, M. G., Erdik, M., Çaktı, E., 2010, "Temporary Earthquake Retrofit of the Land Walls in Istanbul", *In 14th European Conference on Earthquake Engineering*, Ohrid, Republic of Macedonia, 30 August – 3 September 2010.

KOERI, *Boğaziçi University Kandilli Observatory and Earthquake Research Institute, Earthquake Catalogue,* 2019, http://www.koerı.boun.edu.tr/sısmo/zeqdb/.

Komar, D.A., Davy-Jow, S., Decker, S.J., 2012, "The Use of a 3-D Laser Scanner to Document Ephemeral Evidence at Crime Scenes and Postmortem Examinations", *J.*

Forensic Sci, January 2012, Vol. 57, No.1, DOI: 10.1111/j. 1556 – 4029.2011.01915.x.

Kurt, O., 2010, *Deformasyon Analizi*, Ders Notları, KOÜ-Harita Mühendisliği Bölümü, Kocaeli.

Lague, D., Brodu, N., Leroux, J., 2013, "Accurate 3D Comparison of Complex Topography with Terrestrial Laser Scanner: Application to the Rangitikei Canyon (NZ)", *ISPRS Journal of Photogrammetry and Remote Sensing*, 82, pp. 10-26.

Lam S. Y. W., 2006, "Application of Terrestrial Laser Scanning Methodology in Geometric Tolerances Analysis of Tunnel Structures", *Tunneling and Underground Space* Technology, 21(2006) 410.

Lee, J. S., Hong, S. H., Park, I. S., Cho, H. S., Sohn, H. G., 2016, "Evaluation of Geometric Error Sources for Terrestrial Laser Scanner", *Journal of the Korean Society for Geospatial Information Science*, 24(2), pp. 79-87.

Lemy, F., Yong, S., Schulz, T., 2006, "A Case Study of Monitoring Tunnel Wall Displacement Using Laser Scanning Technology", *In Proceedings of IAEG*, Nottingham.

Lindenbergh, R., Pfeifer, N., 2005, "A Statistical Deformation Analysis of Two Epochs of Terrestrial Laser Data of a Lock", *In Proceedings of the 7th Conference on Optical*, pp. 61-70.

Lovse, J. W., Teskey, W. F., Lachapelle, G., Cannon, M. E., 1995, "Dynamic Deformation Monitoring of Tall Structure Using GPS Technology", *Journal of surveying engineering*, *121*(1), pp. 35-40.

Low, K. L., 2004, *Linear Least-Squares Optimization for Point-to-Plane ICP Surface Registration*, Chapel Hill, University of North Carolina, 4(10), pp. 1-3.

Mataija, M., Pogarčic, M., Pogarčic, I., 2014, "Helmert Transformation of Reference Coordinating Systems for Geodesic Purposes in Local Frames", *Procedia Engineering*, 69, pp. 168-176.

Meng, X., Roberts, G. W., Dodson, A. H., Ince, S., Waugh, S., 2006, "GNSS for Structural Deformation and Deflection Monitoring: Implementation and Data Analysis", *In Proceedings of the 3rd IAG/12th FIG Symposium*, Baden, Germany, pp. 22-24.

Mill, T., Alt, A., Liias, R., 2013, "Combined 3D Building Surveying Techniques – Terrestrial Laser Scanning (TLS) and Total Station Surveying for BIM Data Management Purposes", *Journal of Civil Engineering and Management*, 19(sup1), pp. S23-S32.

Milli, T., Ellmann, A., 2014, "Terrestrial Laser Scanning Technology for Deformation Monitoring of a Large Suspension Roof Structure", *In INGEO 2014 – 6th International Conference on Engineering Surveying*, Prague, Czech Republic, April 3-4, 2014.

Moore, J. F. A., 1992, *Monitoring building structures*, J. F. Moore (Ed.). Blackie.

Mostafa Abdel-Bary Ebrahim, 2011, *3D Laser Scanners: History, Applications and Future, Review Article*, Civil Engineering Department, Faculty of Engineering, Assiut University, 2011.

Oliveira, C. S., Çaktı, E., Stengel, D., Branco, M., 2012, "Minaret Behavior Under Earthquake Loading: The Case of Historical Istanbul", *Earthquake Engineering and Structural Dynamics*, 41(1), pp. 19-39.

Oncel, A. O., Wilson, T., 2006, "Evaluation of Earthquake Potential Along the Northern Anatolian Fault Zone in the Marmara Sea Using Comparisons of GPS Strain and Seismotectonic Parameters", *Tectonophysics*, *418*(3-4), pp. 205-218.

Özdoğan, M. V., Deliormanli, A. H., 2018, "Yersel Lazer Tarayıcı ile Yeraltı Galerisinde Meydana Gelen Deformasyonların Belirlenmesi", *Dokuz Eylül Üniversitesi Mühendislik Fakültesi Fen ve Mühendislik Dergisi*, 20(59), pp. 663-675.

Ozener, H., Bulut, F., Aktug, B., Yaltirak, C., Dogru, A., 2018, "Slip Deficit on the North Anatolian Fault: Implications for Pending Earthquakes Offshore Istanbul", *AGUFM,* 2018, S44A-08.

Park, H., Lee, D., 2019, "Comparison Between Point Cloud and Mesh Models Using Images from an Unmanned aerial Vehicle", *Measurement*, 138 (2019), pp. 461 – 466.

Pellegrinelli, A., Furini, A., Russo, P., 2014, Earthquakes and ancient leaning towers: Geodetic monitoring of the bell tower of San Benedetto Church in Ferrara (Italy), Journal of Cultural Heritage 15.6 (2014): 687-691.

Pesci, A., Bonali, E., Galli, C., Boschi, E., 2012, "Laser Scanning and Digital Imaging for the Investigation of an Ancient Building: Palazzo d'Accursio Study Case Bologna, Italy", *Journal of Cultural Heritage*, 13 (2012, pp. 215–220.

Pınar, N., Lahn, E, 1952, *Turkish Earthquake Catalog with Descriptions*, Technical Report, Turkey the Ministry of Public Works and Settlement, The General Directorate of Construction Affairs, Serial 6, no. 36.

Pomerleau, F., Colas, F., Siegwart, R., 2015, "A Review of Point Cloud Registration Algorithms for Mobile Robotics", *Foundations and Trends® in Robotics*, 4(1), pp. 1-104.

Reshetyuk, Y., 2009, *Self-Calibration and Direct Georeferencing in Terrestrial Laser Scanning*, Doctoral Dissertation, KTH.

Romsek, B.R., 2008, *Terrestrial Laser Scanning: Comparison of Time-of-Flight and Phase-Based Measuring Systems*, Master Thesis, Purdue University.

Rosser, N. J., Petley, D.N., Lim, M., Dunning, S.A., Allison, R.J., 2005, "Terrestrial Laser Scanning for Monitoring the Process of Hard Rock Coastal Cliff Erosion", *Quarterly Journal of Engineering Geology and Hydrogeology*, 38(4), pp. 363-375. DOI:10.1144/1470-9236/05-008.

Rusinkiewicz, S., Levoy, M., 2001, "Efficient Variants of the ICP Algorithm", *In Proceedings Third International Conference on 3-D Digital Imaging and Modeling*, pp. 145-152, IEEE.

SCENE 2019.0 User Manual, January 2019 Version, © FARO Technologies Inc., 2019.

Selbesoglu, M. O., Bakirman, T., Gokbayrak, O., 2016, "Deformation Measurement Using Terrestrial Laser Scanner for Cultural Heritage", *International Archives of the Photogrammetry, Remote Sensing and Spatial Information Sciences*, 42 (2016).

Sengul, A., 2008, "3D GIS Example in Historical Peninsula of Istanbul", *The International Archives of the Photogrammetry, Remote Sensing and Spatial Information Sciences*, 37, pp. 659-664.

Slattery, K.T., Slattery, D.K., Peterson, J.P., 2012, "Road Construction Earthwork Volume Calculation Using Three-Dimensional Laser Scanning", *Journal of Surveying Engineering*, Vol. 138, No. 2, May 1, 2012, DOI: 10.1061/(ASCE)SU.1943-5428.0000073.

Soysal, H., Sipahioğlu, S., Kolçak, D., Altınok, Y., 1981, *Historical Earthquake Catalog of Turkey and Surrounding area (2100 B.C. – 1900 A.D.)*, Technical Report, TÜBİTAK, No. TBAG-341.

Soudarissanane, S., Lindenbergh, R., Gorte, B., 2008, "Reducing the Error in Terrestrial Laser Scanning by Optimizing the Measurement Set-Up", *In XXI ISPRS Congress*, Commission I-VIII, 3-11 July 2008, Beijing, China.

Soudarissanane, S., J. Van Ree, Bucksch, A., Lindenbergh, R., 2007, "Error Budget of Terrestrial Laser Scanning: Influence of the Incident Angle on the Scan Quality", *In Proceedings 3D-NordOs*, pp. 1-8.

Stephanie, K., Schwieger, V., 2017, "A Synthetic Covariance Matrix for Monitoring by Terrestrial Laser Scanning", *J. Appl. Geodesy*, 11(2), pp. 77-87.

Suchocki, C., Katzer, J., 2018, "Terrestrial Laser Scanning Harnessed for Moisture Detection in Building Materials – Problems and Limitations", *Automation in Construction*, 94 (2018), pp. 127–134.

Temizer, T., Nemli, G., Ekizce, E., Ekizce, A., Demir, S., Bayram, B., Yilmaz, H. F., 2013, "3D Documentation of a Historical Monument Using Terrestrial Laser Scanning Case Study: Byzantine Water Cistern, Istanbul", *International Archives of the Photogrammetry, Remote Sensing and Spatial Information Sciences*, 5, W2.

Teza, G., Galgaro, A., Zaltron, N., Genevois, R., 2007, "Terrestrial Laser Scanner to Detect Landslide Displacement Fields: A New Approach", *International Journal of Remote Sensing*, Volume 28, Issue 16, January 2007, pp. 3426-2446.

Thagunna, G., 2014, "Building Cracks – Causes and Remedies", *In 3rd World Conference on Applied Sciences, Engineering and Technology*, at Basha Research Centre.

Tsakiri, M., Lichti, D., Pfeifer, N., 2006, "Terrestrial Laser Scanning for Deformation Monitoring".

Turnbull, S., *The Walls of Constantinople AD 324 – 1453*, Bloomsbury Publishing, 2012.

Uray, F., Metin, A., Varlik, A., 2015, "3D Architectural Surveying of Diyarbakir Wall's Ulu Beden Tower with Terrestrial Laser Scanner", *In World Multidisciplinary Earth Science Symposium*, WMESS, 2015.

USACE, 2002, *Engineering and Design: Structural Deformation Surveying*, No. 1110-2-1009, Washington, DC: Department of the Army-US Army Corps of Engineers.

Ündül, Ö., Tuğrul, A., 2006, "The Engineering Geology of İstanbul, Turkey", *In Proceedings of the 10th IAEG International Congress*, Paper No. 392, pp. 6-10.

Vacca, G., Mistretta, F., Stochino, F., Dessi, A., 2016, "Terrestrial Laser Scanner for Monitoring the Deformations and the Damages of Buildings", *International Archives of the Photogrammetry, Remote Sensing and Spatial Information Sciences*, 41.B5 (2016), pp. 453-460.

Van Goor, B., 2011, *Change Detection and Deformation Analysis Using Terrestrial Laser Scanning: Case Study of the Metro Tunnel at Rotterdam Central Station*, Master's Thesis, Delft University of Technology.

Vasilakos, C., Chatzistamatis, S., Roussou, O., Soulakellis, N., 2018, "Terrestrial Photogrammetry vs Laser Scanning for Rapid Earthquake Damage Assessment", *The International Archives of the Photogrammetry, Remote Sensing and Spatial Information Sciences*, Volume XLII-3/W4, 2018 GeoInformation For Disaster Management (Gi4DM), 18–21 March 2018, Istanbul, Turkey.

Wessel, P., Smith, W. H. F., Scharroo, R., Luis, J., Wobbe, F., 2013, "Generic Mapping Tools: Improved Version Released", *EOS Trans. AGU, 94(45)*, p. 409 – 410, 2013. doi:10.1002/2013EO45001.

Xu, H., Li, H., Yang, X., Qi, S., Zhou, J., 2019, "Integration of Terrestrial Laser Scanning and NURBS Modeling for the Deformation Monitoring of an Earth-Rock Dam", *Sensors*, *19*(1), p. 22.

Yaman, A., 2013, *Yersel Lazer Tarayıcıların Tarama Açısı ve Mesafesine Bağlı Olarak Konum Doğruluğunun Araştırılması*, Yüksek Lisans Tezi, Aksaray Üniversitesi.

Yanik, H. B., Flores, A., 2009, “Understanding Rigid Geometric Transformations: Jeff's Learning Path for Translation”, *The Journal of Mathematical Behavior*, 28(1), pp. 41-57.

Zhang, Z., 1994, “Iterative Point Matching for Registration of Free-Form Curves and Surfaces”, *International Journal of Computer Vision*, 13(2), pp. 119-152.